

# Electronic Supplementary Information

for

**Vibronic effects accelerate the intersystem crossing processes of the  
through-space charge transfer states in the triptycene bridged  
acridine-triazine donor-acceptor molecule TpAT-tFFO**

Jeremy M. Kaminski,<sup>a</sup> Angela Rodríguez-Serrano,<sup>a</sup> Fabian Dinkelbach,<sup>a</sup>  
Hector Miranda-Salinas,<sup>b</sup> Andrew P. Monkman<sup>b</sup> and Christel M. Marian<sup>\*a</sup>

<sup>a</sup> Institute of Theoretical and Computational Chemistry,  
Heinrich-Heine-University Düsseldorf, Universitätsstraße 1,  
D-40225 Düsseldorf, Germany, E-mail: christel.marian@hhu.de

<sup>b</sup> OEM research group, Dept. of Physics, Durham University,  
Durham, UK, DH1 3LE, E-mail: a.p.monkman@durham.ac.uk

20.12.2021

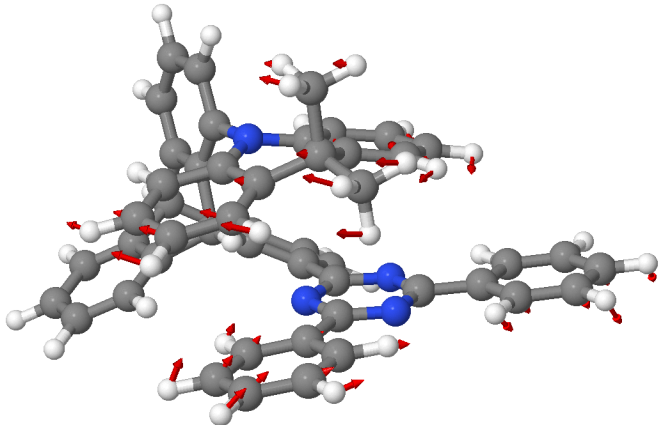


Figure S1: Vibrational mode 1 at the  $S_0(\text{Me} \rightarrow \text{N})$  geometry in vacuo.

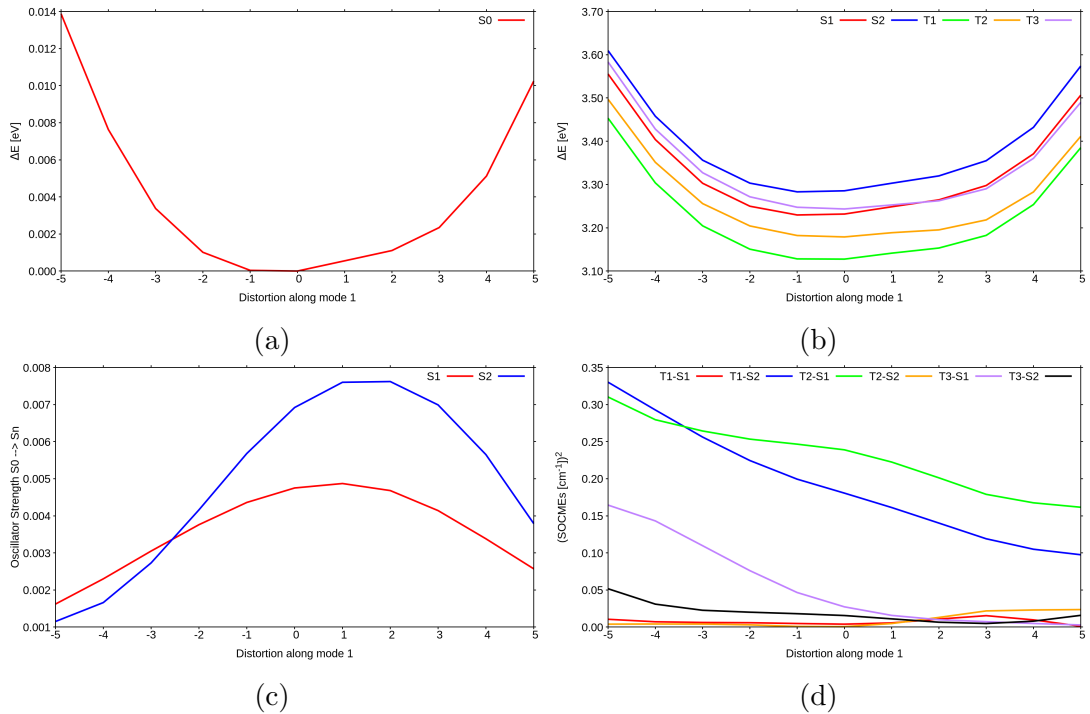


Figure S2: Scan along vibrational mode 1: (a) Relative DFT/MRCI ground state energy differences w.r.t. the undistorted  $S_0(\text{Me} \rightarrow \text{N})$  geometry, (b) DFT/MRCI excitation energies w.r.t. the ground state energy at the undistorted  $S_0(\text{Me} \rightarrow \text{N})$  geometry, (c) oscillator strengths for the  $S_0 \rightarrow S_1$  and  $S_0 \rightarrow S_2$  absorption processes, (d) sum of the squared SOCMEs for transitions discussed in this study.

Table S1: DFT/MRCI-R2016 vertical excitation energies and characterization of low-lying singlet and triplet states of **TpAT-tFFO** calculated at the  $S_0(\text{Me} \rightarrow \text{N})$  geometry.

State	$\Delta E$ [eV]	f(L)	Transition	Character	%	$\mu$ [D]
S <sub>0</sub>	0.02		GS		96	0.61
S <sub>1</sub>	3.25	0.005	H → L	CT	68	16.24
			H → L+1		21	
S <sub>2</sub>	3.30	0.007	H → L+1	CT'	67	16.42
			H → L		21	
T <sub>1</sub>	3.14		H → L	CT	70	15.37
			H → L+1		16	
T <sub>2</sub>	3.19		H → L+1	CT'	67	14.43
			H → L		14	
T <sub>3</sub>	3.24		H-5 → L	LE	25	0.39
			H-6 → L		13	

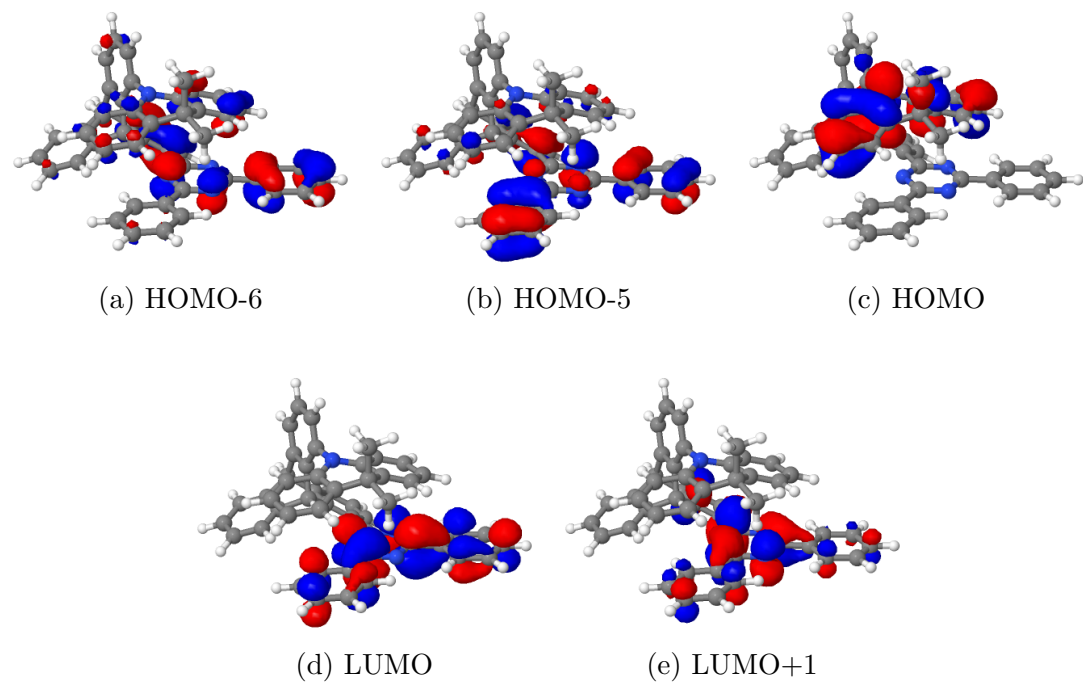


Figure S3: BH-LYP molecular orbitals (cutoff 0.03) at the  $S_0$ (Me $\rightarrow$ N) geometry in vacuo.

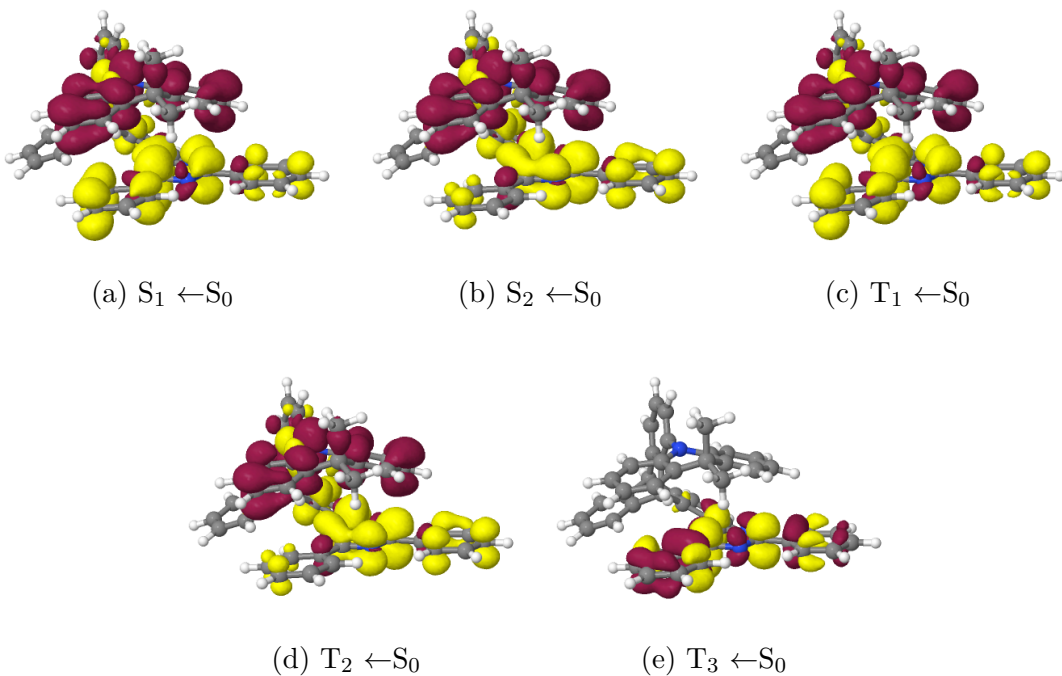


Figure S4: Difference densities ( $\pm 0.001$ ) of the excited states at the  $S_0(\text{Me} \rightarrow \text{N})$  geometry in vacuo. Areas losing electron density in comparison to the electronic ground state are shown in red, areas gaining electron density in yellow.

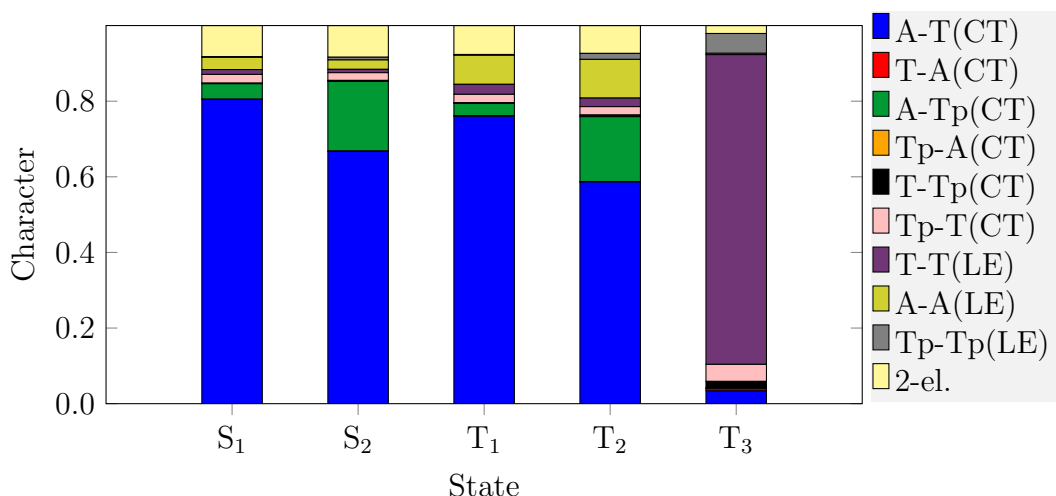


Figure S5: Fragment-based analysis for the vertical singlet and triplet state DFT/MRCI-R2016 wavefunctions at the  $S_0(\text{Me} \rightarrow \text{N})$  geometry in vacuo.

Table S2: DFT/MRCI-R2016 vertical excitation energies and characterization of low-lying singlet and triplet states of **TpAT-tFFO** calculated at the  $S_0$ (Me $\rightarrow$ Ph) geometry.

State	$\Delta E$ [eV]	f(L)	Transition	Character	%	$\mu$ [D]
$S_0$	0.00		GS		96	0.65
$S_1$	3.27	0.002	H $\rightarrow$ L+1	CT	49	16.72
			H $\rightarrow$ L		39	
$S_2$	3.33	0.000	H $\rightarrow$ L	CT'	48	18.50
			H $\rightarrow$ L+1		39	
$T_1$	3.17		H $\rightarrow$ L	CT	71	14.41
$T_2$	3.17		H $\rightarrow$ L+1	CT'	56	9.93
			H-5 $\rightarrow$ L+1		10	
$T_3$	3.29		H $\rightarrow$ L+1	LE/CT	29	6.93
			H-6 $\rightarrow$ L		17	
			H-4 $\rightarrow$ L		10	

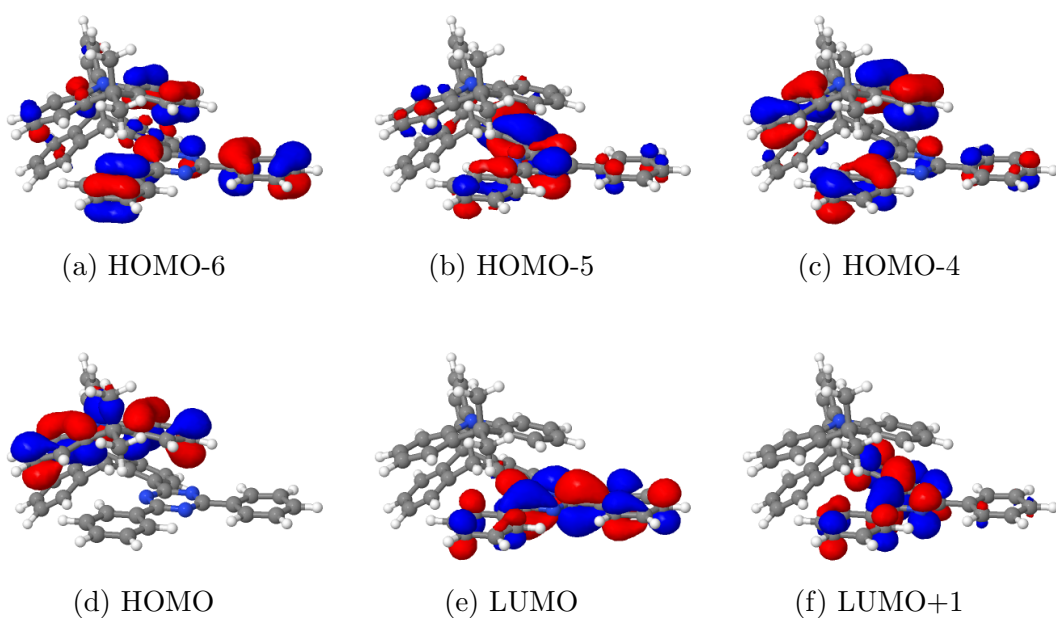


Figure S6: BH-LYP molecular orbitals (cutoff 0.03) at the  $S_0$ (Me $\rightarrow$ Ph) geometry in vacuo.

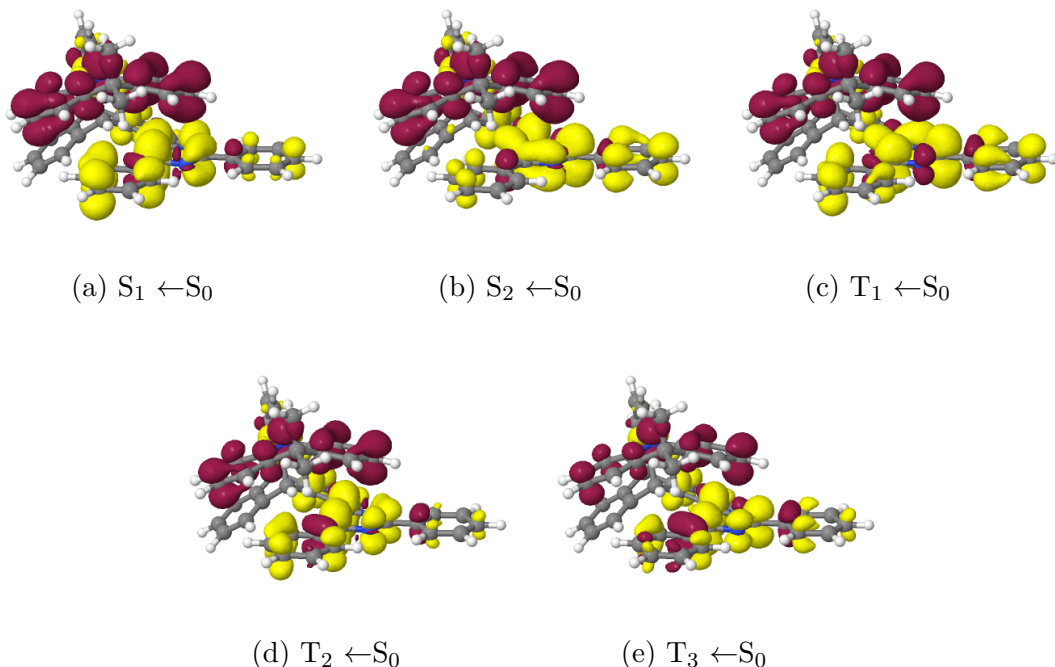


Figure S7: Difference densities ( $\pm 0.001$ ) of the excited states at the  $S_0$ (Me $\rightarrow$ Ph) geometry in vacuo. Areas losing electron density in comparison to the electronic ground state are shown in red, areas gaining electron density in yellow.

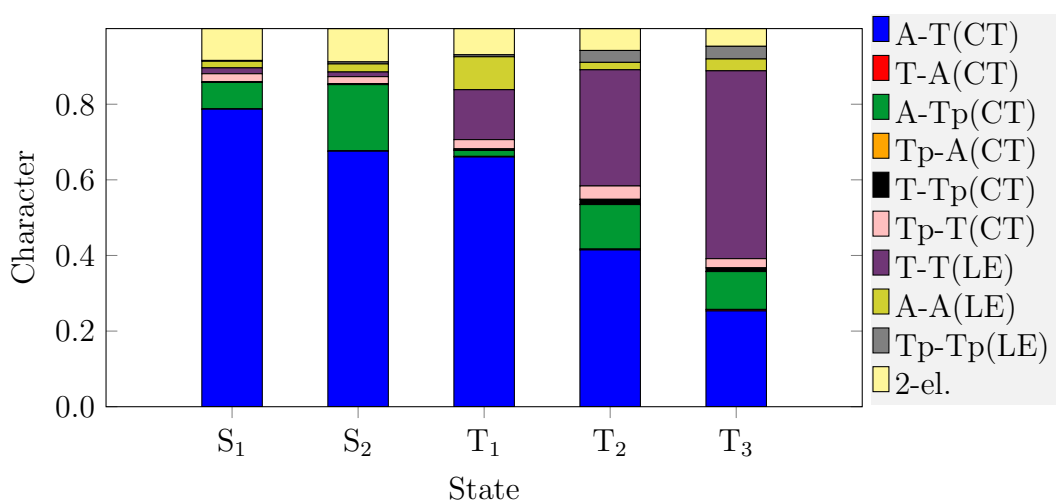


Figure S8: Fragment-based analysis for the vertical singlet and triplet state DFT/MRCI-R2016 wavefunctions at the  $S_0(\text{Me} \rightarrow \text{Ph})$  geometry in vacuo.

Table S3: DFT/MRCI-R2016 vertical excitation energies and characterization of low-lying singlet and triplet states of **TpAT-tFFO** calculated at the  $S_1$  geometry.

State	$\Delta E$ [eV]	Transition	Character	%	$\mu$ [D]
$S_0$	0.41	GS		96	0.45
$S_1$	2.97	H $\rightarrow$ L	CT	90	15.65
$S_2$	3.51	H $\rightarrow$ L+1	CT'	88	15.65
$T_1$	2.89	H $\rightarrow$ L	CT	89	15.40
$T_3$	3.29	H-5 $\rightarrow$ L	LE	25	1.49
		H-2 $\rightarrow$ L		15	
		H-9 $\rightarrow$ L		14	
$T_2$	3.42	H $\rightarrow$ L+1	CT'	83	14.41

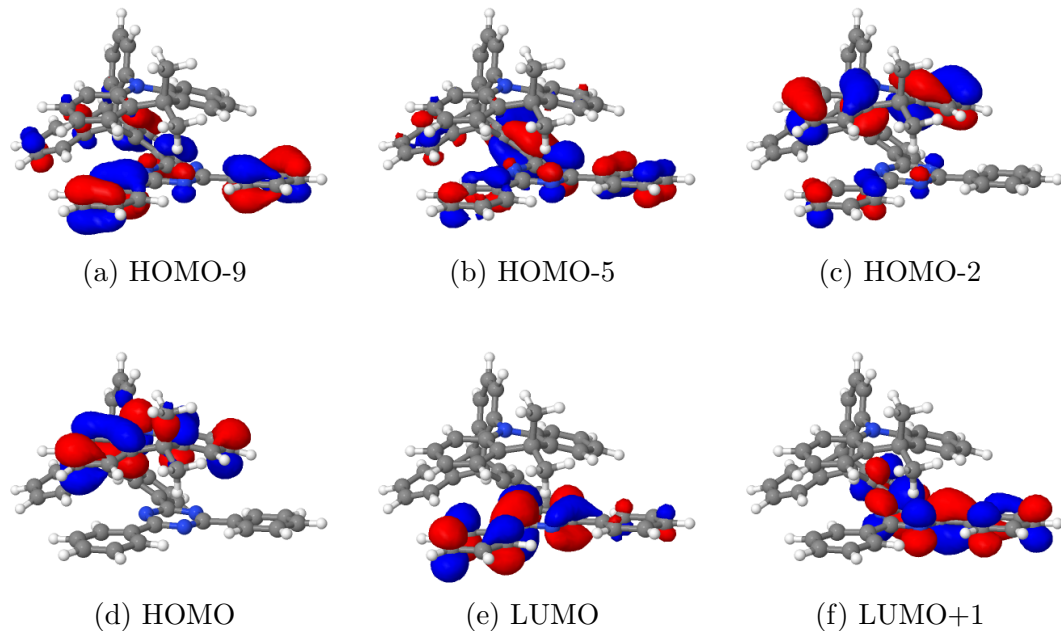


Figure S9: BH-LYP molecular orbitals (cutoff 0.03) at the  $S_1$  geometry in vacuo.

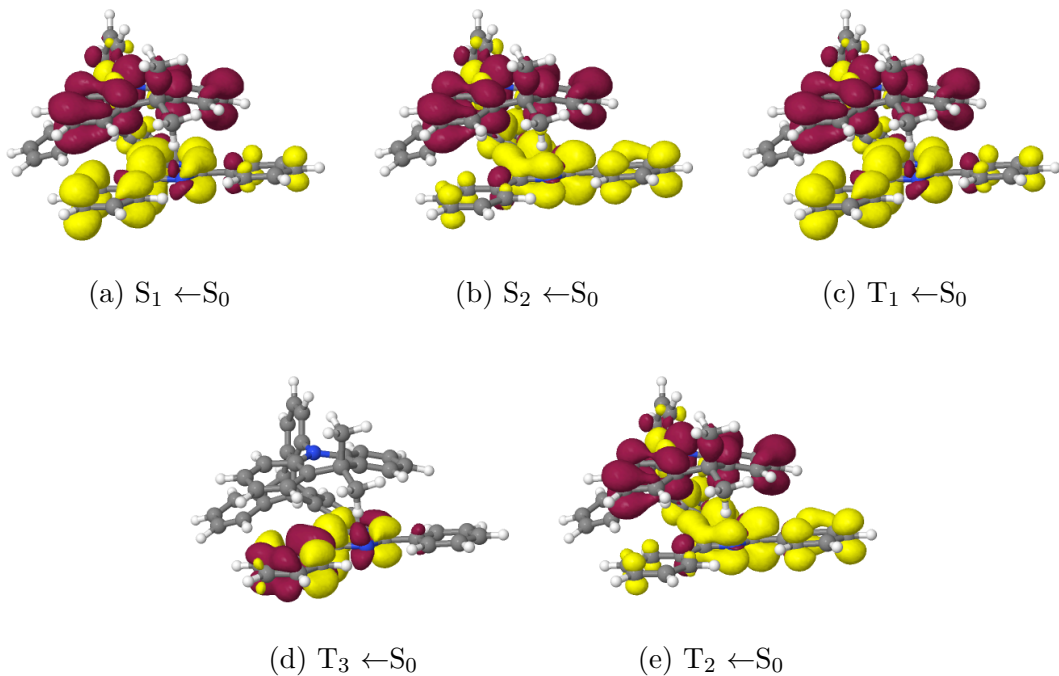


Figure S10: Difference densities ( $\pm 0.001$ ) of the excited states at the  $S_1$  geometry in vacuo. Areas losing electron density in comparison to the electronic ground state are shown in red, areas gaining electron density in yellow.

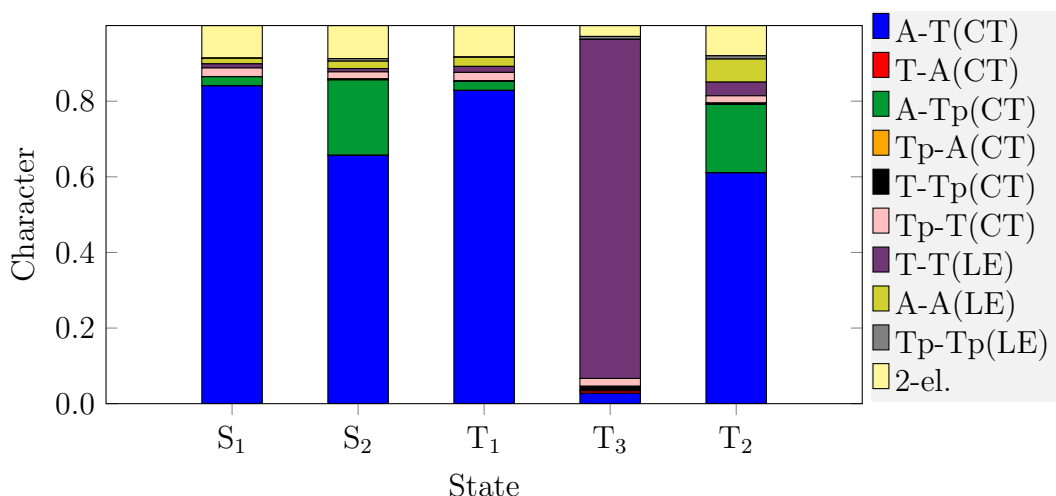


Figure S11: Fragment-based analysis for the vertical singlet and triplet state DFT/MRCI-R2016 wavefunctions at the  $S_1$  geometry in vacuo.

Table S4: DFT/MRCI-R2016 vertical excitation energies and characterization of low-lying singlet and triplet states of **TpAT-tFFO** calculated at the  $S_2$  geometry.

State	$\Delta E$ [eV]	Transition	Character	%	$\mu$ [D]
$S_0$	0.38	GS		96	1.08
$S_2$	2.98	H $\rightarrow$ L	CT'	88	18.39
$S_1$	3.47	H $\rightarrow$ L+1	CT	88	14.92
$T_2$	2.86	H $\rightarrow$ L	CT'	83	16.77
$T_3$	3.30	H-6 $\rightarrow$ L H-9 $\rightarrow$ L	LE	32 16	2.00
$T_1$	3.38	H $\rightarrow$ L+1	CT	76	12.63

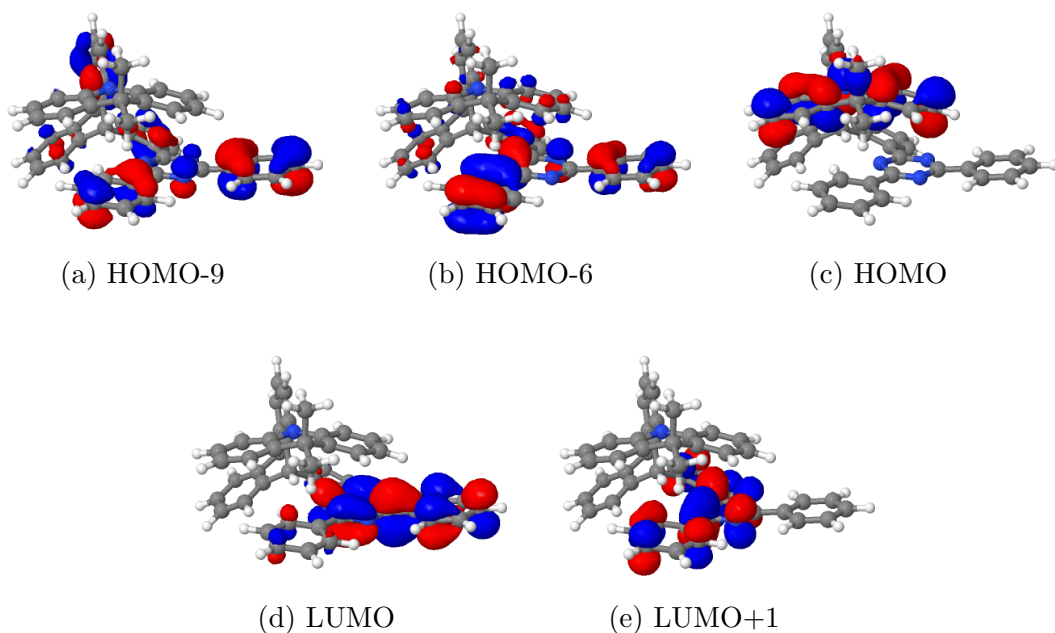


Figure S12: BH-LYP molecular orbitals (cutoff 0.03) at the  $S_2$  geometry in vacuo.

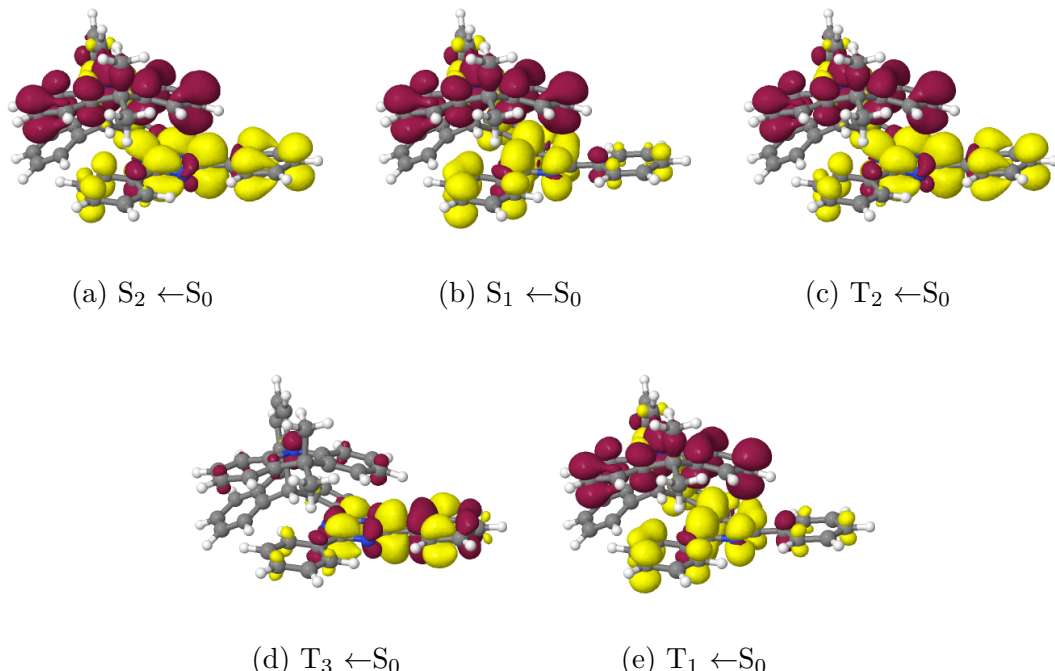


Figure S13: Difference densities ( $\pm 0.001$ ) of the excited states at the  $S_2$  geometry in vacuo. Areas losing electron density in comparison to the electronic ground state are shown in red, areas gaining electron density in yellow.

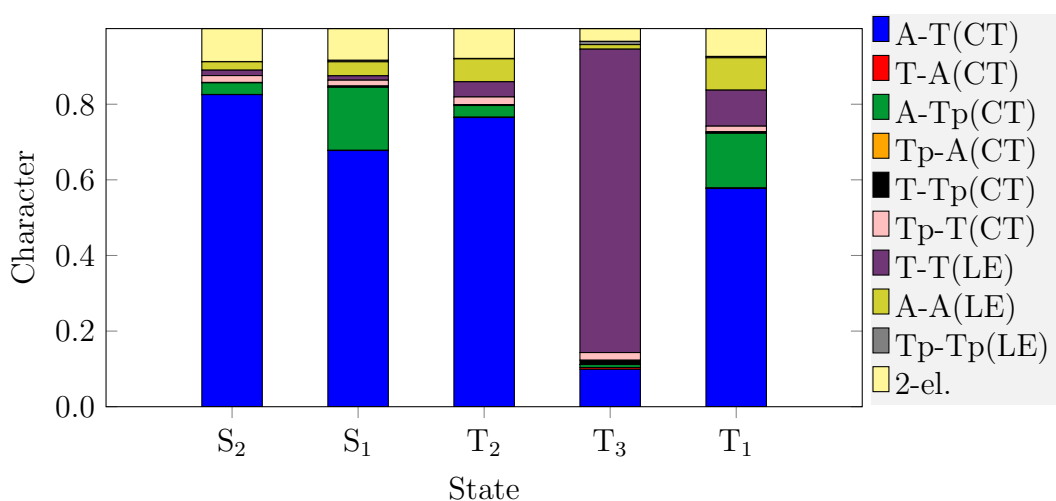


Figure S14: Fragment-based analysis for the vertical singlet and triplet state DFT/MRCI-R2016 wavefunctions at the  $S_2$  geometry in vacuo.

Table S5: DFT/MRCI-R2016 vertical excitation energies and characterization of low-lying singlet and triplet states of **TpAT-tFFO** calculated at the T<sub>1</sub> geometry.

State	$\Delta E$ [eV]	Transition	Character	%	$\mu$ [D]
S <sub>0</sub>	0.40	GS		96	0.43
S <sub>1</sub>	2.96	H → L	CT	90	15.40
S <sub>2</sub>	3.48	H → L+1	CT'	88	15.45
T <sub>1</sub>	2.88	H → L	CT	89	15.11
T <sub>3</sub>	3.29	H-5 → L H-2 → L H-9 → L	LE	27 20 14	1.51
T <sub>2</sub>	3.38	H → L+1	CT'	83	14.18

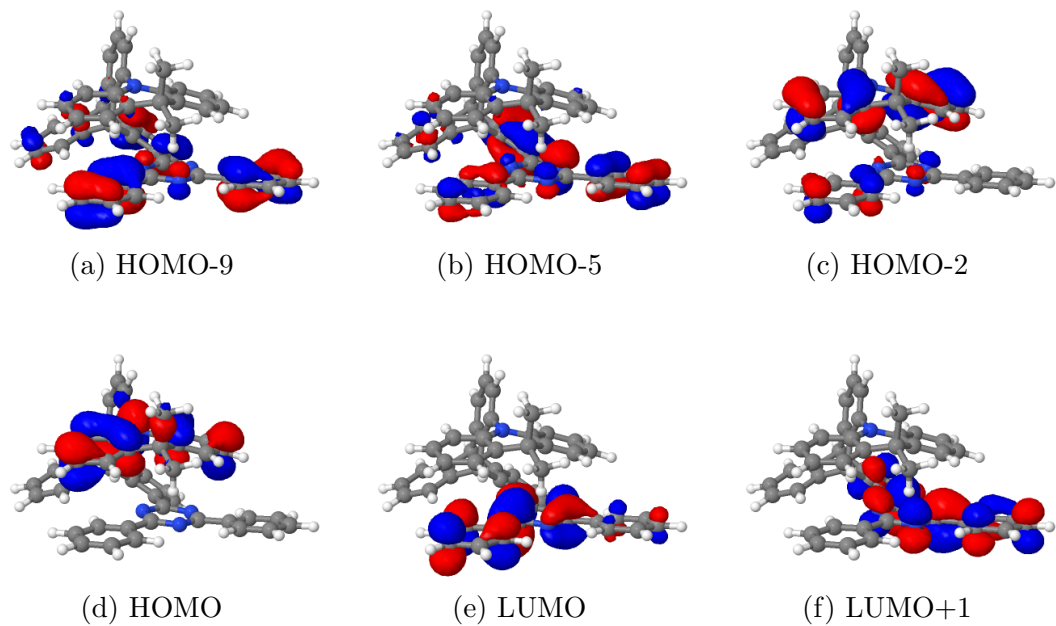


Figure S15: BH-LYP molecular orbitals (cutoff 0.03) at the T<sub>1</sub> geometry in vacuo.

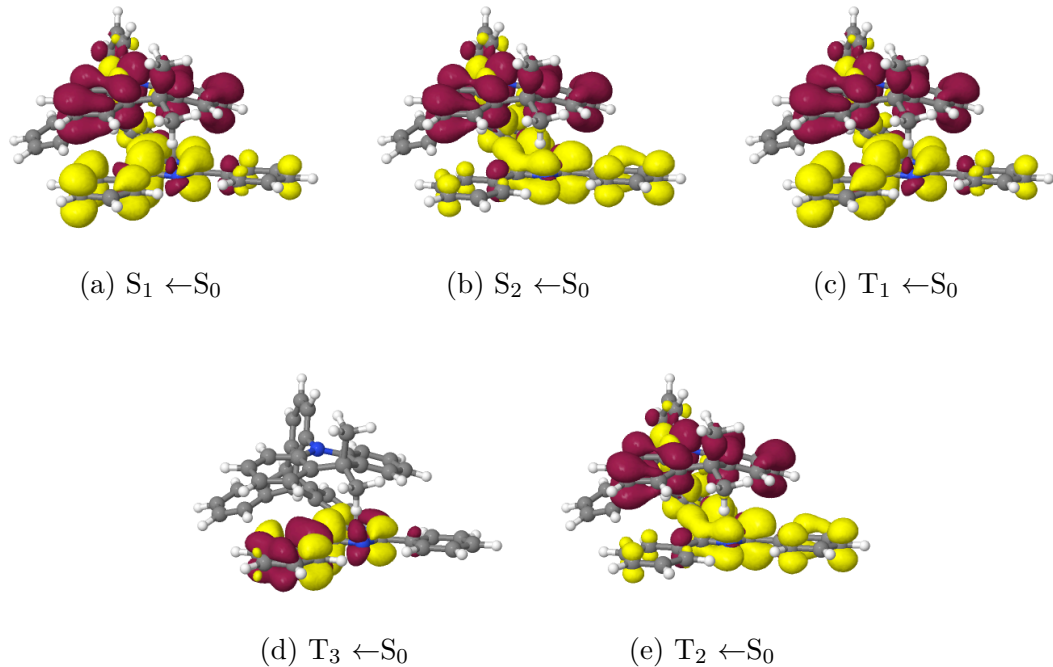


Figure S16: Difference densities ( $\pm 0.001$ ) of the excited states at the T<sub>1</sub> geometry in vacuo. Areas losing electron density in comparison to the electronic ground state are shown in red, areas gaining electron density in yellow.

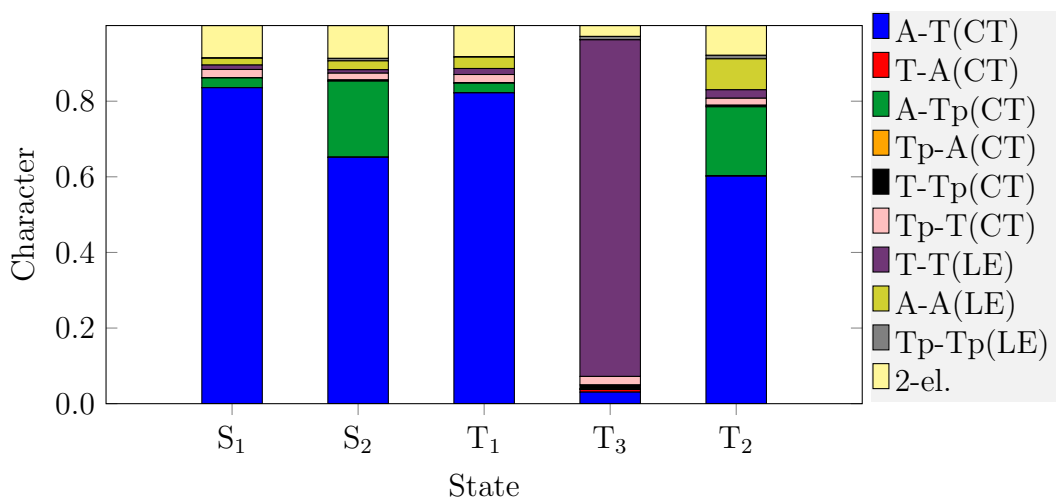


Figure S17: Fragment-based analysis for the vertical singlet and triplet state DFT/MRCI-R2016 wavefunctions at the T<sub>1</sub> geometry in vacuo.

Table S6: DFT/MRCI-R2016 vertical excitation energies and characterization of low-lying singlet and triplet states of **TpAT-tFFO** calculated at the CI geometry.

State	$\Delta E$ [eV]	Transition	Character	%	$\mu$ [D]
$S_0$	0.24	GS		96	0.87
$S_2$	3.08	$H \rightarrow L+1$	CT	67	14.54
		$H \rightarrow L$		21	
$S_1$	3.10	$H \rightarrow L$	CT'	67	16.49
		$H \rightarrow L+1$		22	
$T_2$	2.99	$H \rightarrow L+1$	CT	69	13.80
		$H \rightarrow L$		17	
$T_1$	2.99	$H \rightarrow L$	CT'	67	15.58
		$H \rightarrow L+1$		18	
$T_3$	3.36	$H-5 \rightarrow L+1$	LE	25	0.33
		$H-6 \rightarrow L$		20	
		$H-2 \rightarrow L+1$		13	

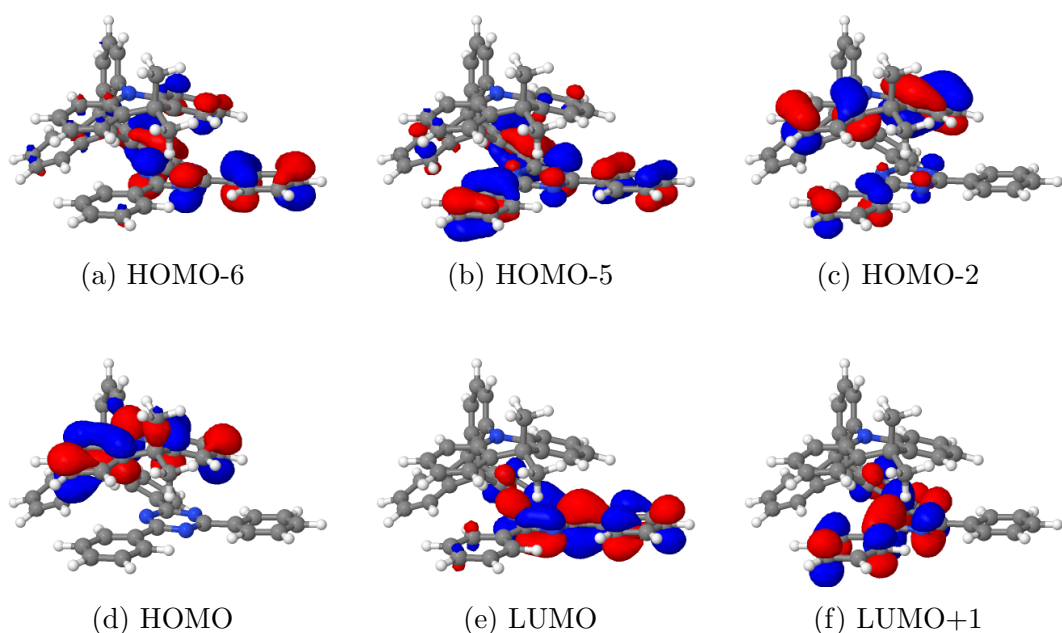


Figure S18: BH-LYP molecular orbitals (cutoff 0.03) at the CI geometry in vacuo.

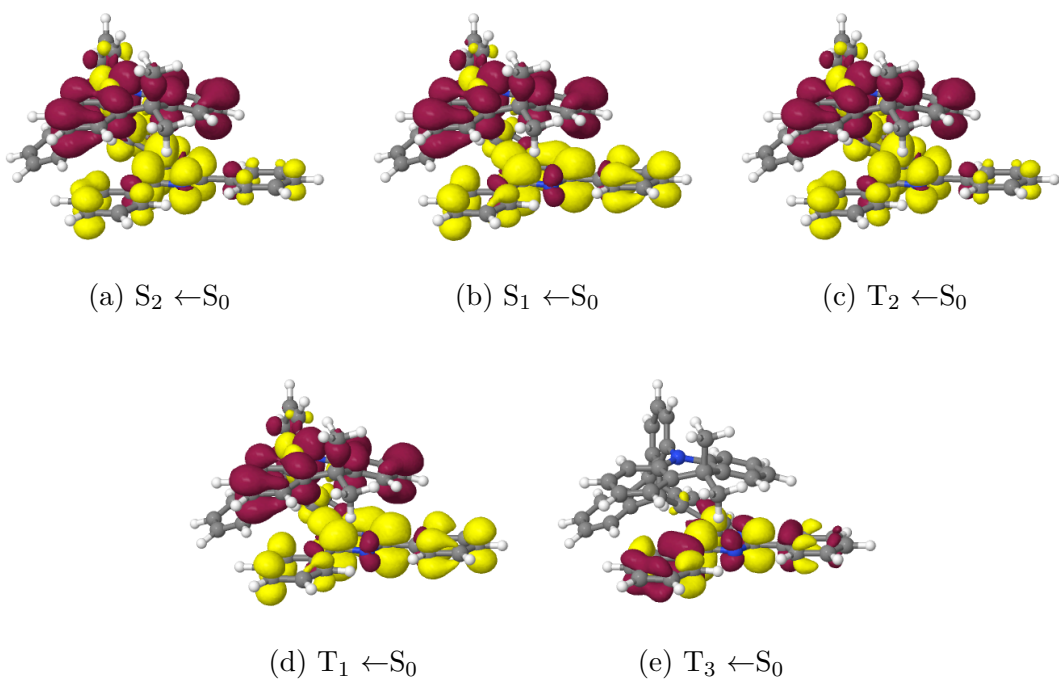


Figure S19: Difference densities ( $\pm 0.001$ ) of the excited states at the CI geometry in vacuo. Areas losing electron density in comparison to the electronic ground state are shown in red, areas gaining electron density in yellow.

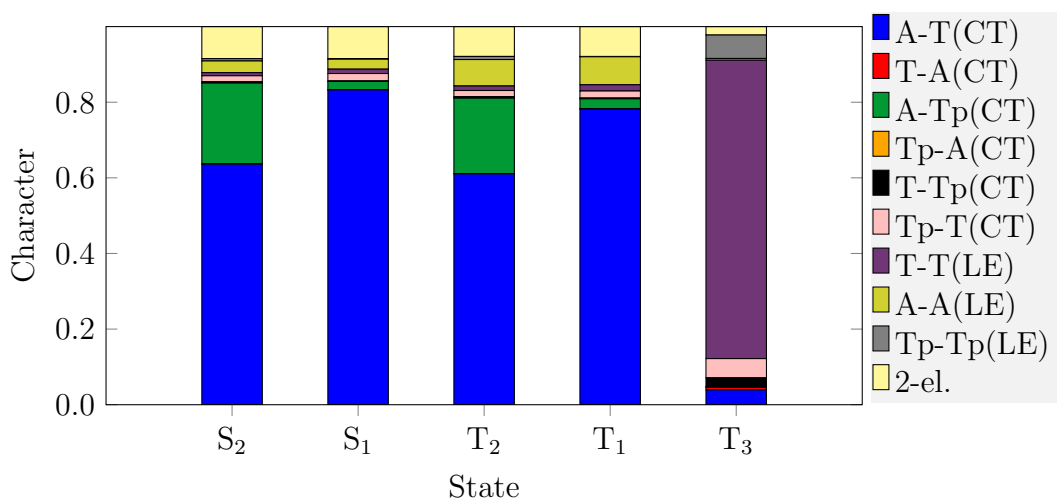


Figure S20: Fragment-based analysis for the vertical singlet and triplet state DFT/MRCI-R2016 wavefunctions at the CI geometry in vacuo.

Table S7: DFT/MRCI-R2016 vertical excitation energies and characterization of low-lying singlet and triplet states of **TpAT-tFFO** calculated at the T<sub>2</sub> geometry.

State	$\Delta E$ [eV]	Transition	Character	%	$\mu$ [D]
S <sub>0</sub>	0.39	GS		96	1.00
S <sub>2</sub>	2.97	H → L	CT'	88	17.77
S <sub>1</sub>	3.45	H → L+1	CT	88	14.47
T <sub>2</sub>	2.83	H → L	CT'	82	15.77
T <sub>1'</sub>	3.32	H → L+1	LE/CT	30	4.78
		H-6 → L		20	
		H-9 → L		10	
T <sub>1''</sub>	3.36	H → L+1	CT/LE	53	8.62
		H-6 → L		12	
		H-9 → L		7	

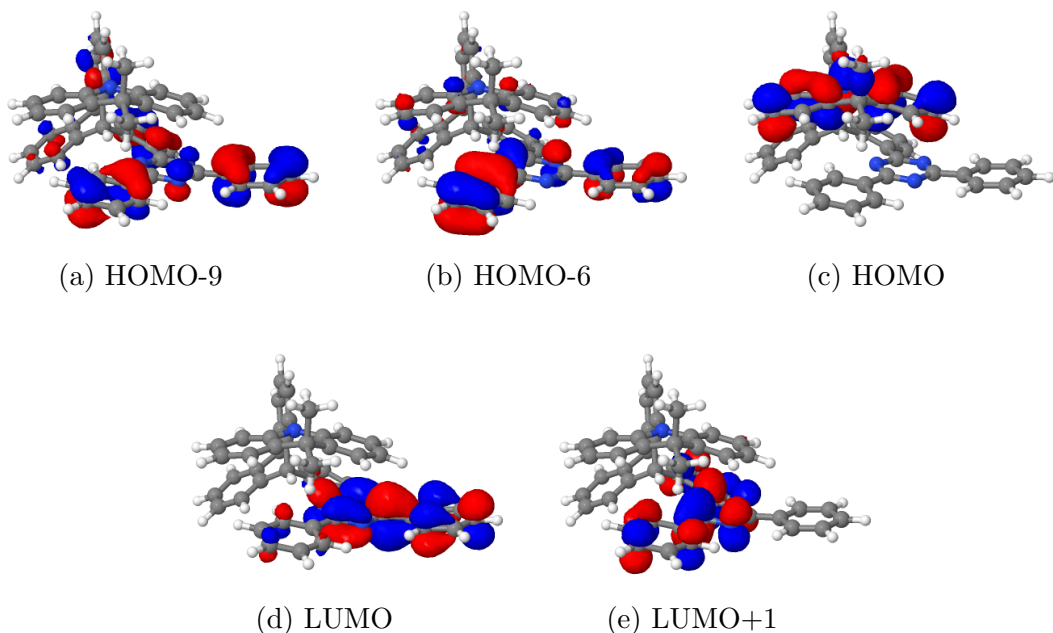


Figure S21: BH-LYP molecular orbitals (cutoff 0.03) at the T<sub>2</sub> geometry in vacuo.

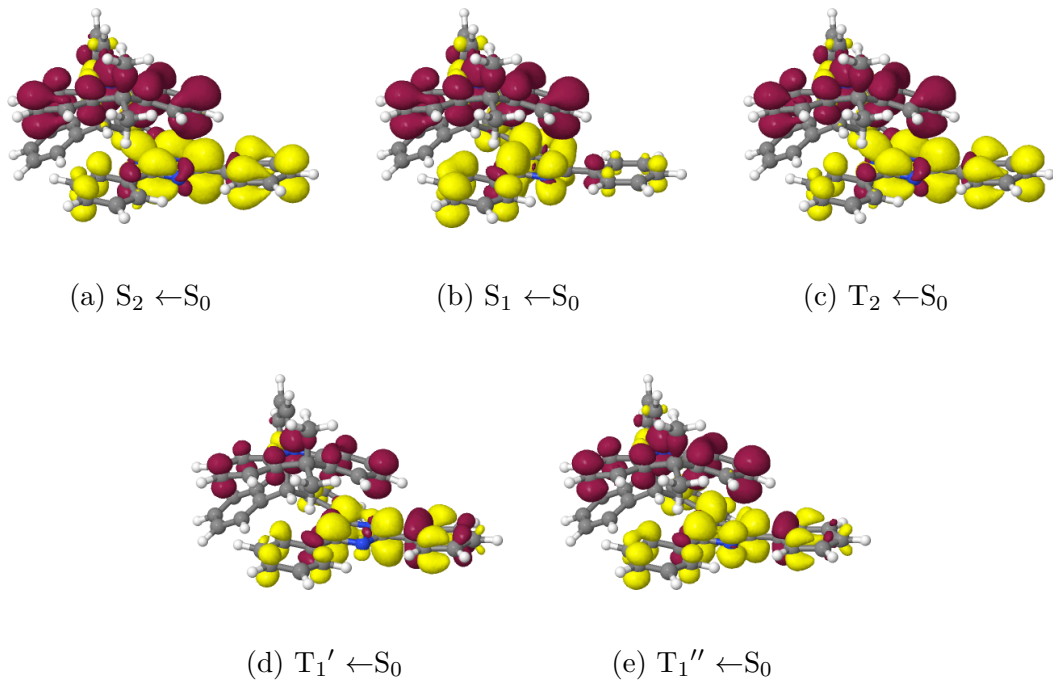


Figure S22: Difference densities ( $\pm 0.001$ ) of the excited states at the T<sub>2</sub> geometry in vacuo. Areas losing electron density in comparison to the electronic ground state are shown in red, areas gaining electron density in yellow.

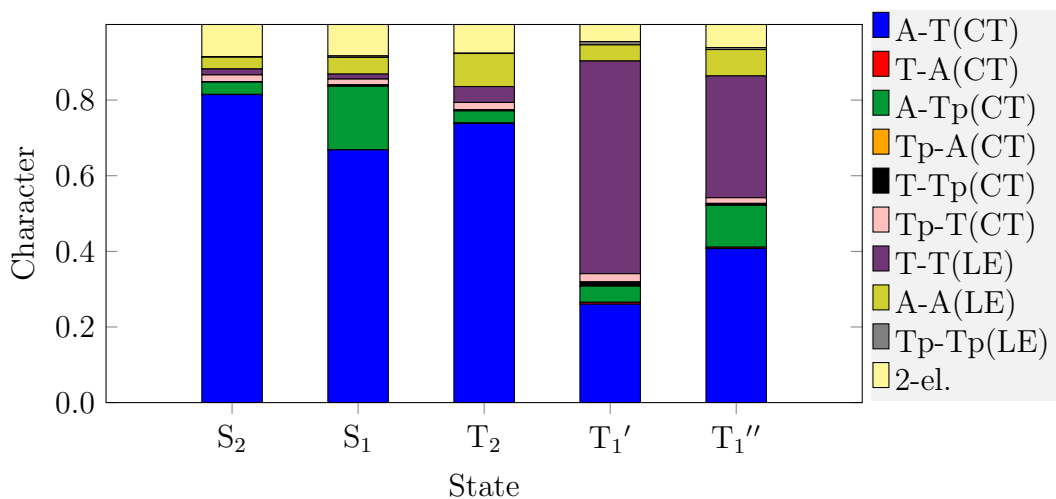


Figure S23: Fragment-based analysis for the vertical singlet and triplet state DFT/MRCI-R2016 wavefunctions at the T<sub>2</sub> geometry in vacuo.

Table S8: DFT/MRCI-R2016 vertical excitation energies and characterization of low-lying singlet and triplet states of **TpAT-tFFO** calculated at the T<sub>3</sub> geometry.

State	$\Delta E$ [eV]	Transition	Character	%	$\mu$ [D]
$S_0$	0.32	GS		96	0.46
$S_1$	3.17	H $\rightarrow$ L	CT	89	15.88
$S_2$	3.58	H $\rightarrow$ L+1	CT'	87	16.00
$T_3$	2.99	H-2 $\rightarrow$ L	LE	35	2.26
		H-4 $\rightarrow$ L		20	
$T_1$	3.08	H $\rightarrow$ L	CT	78	14.09
$T_2$	3.44	H $\rightarrow$ L+1	CT'	78	13.50

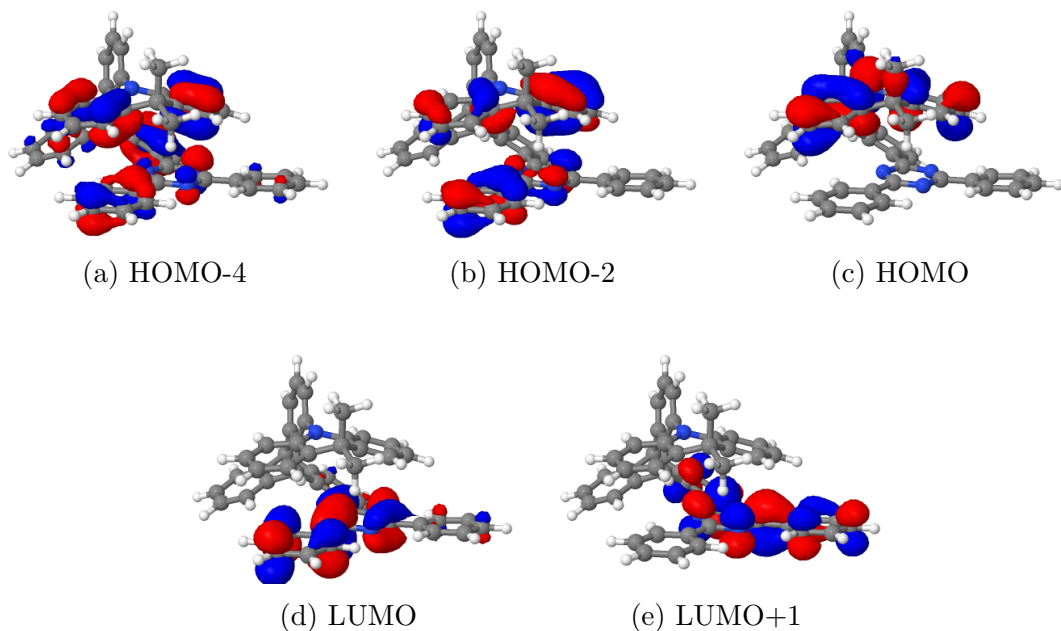


Figure S24: BH-LYP molecular orbitals (cutoff 0.03) at the T<sub>3</sub> geometry in vacuo.

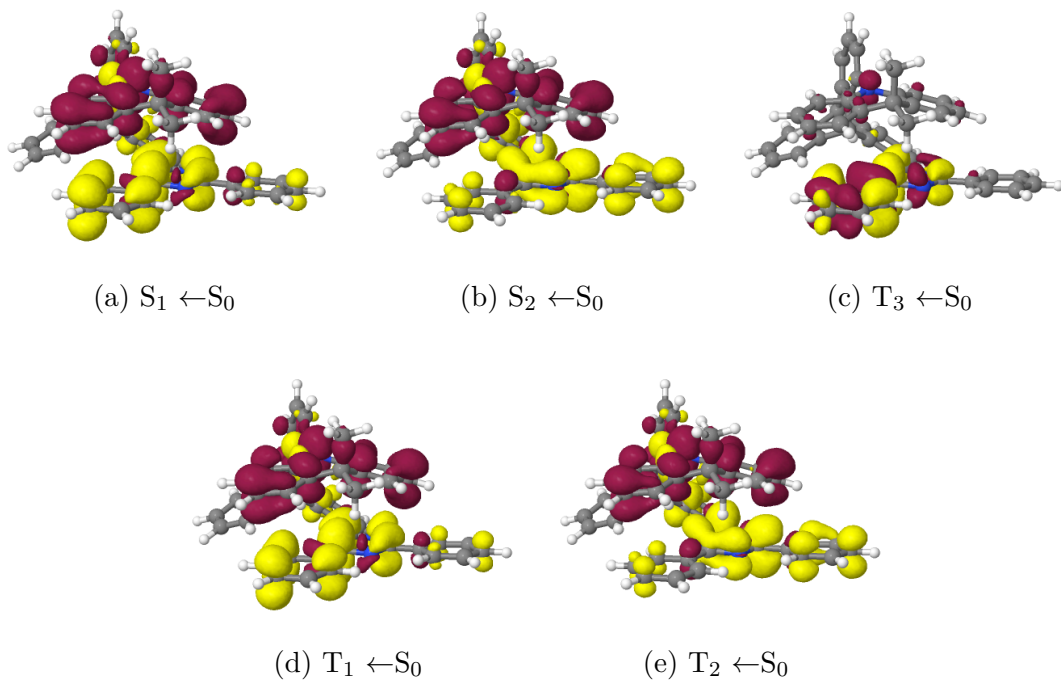


Figure S25: Difference densities ( $\pm 0.001$ ) of the excited states at the T<sub>3</sub> geometry in vacuo. Areas losing electron density in comparison to the electronic ground state are shown in red, areas gaining electron density in yellow.

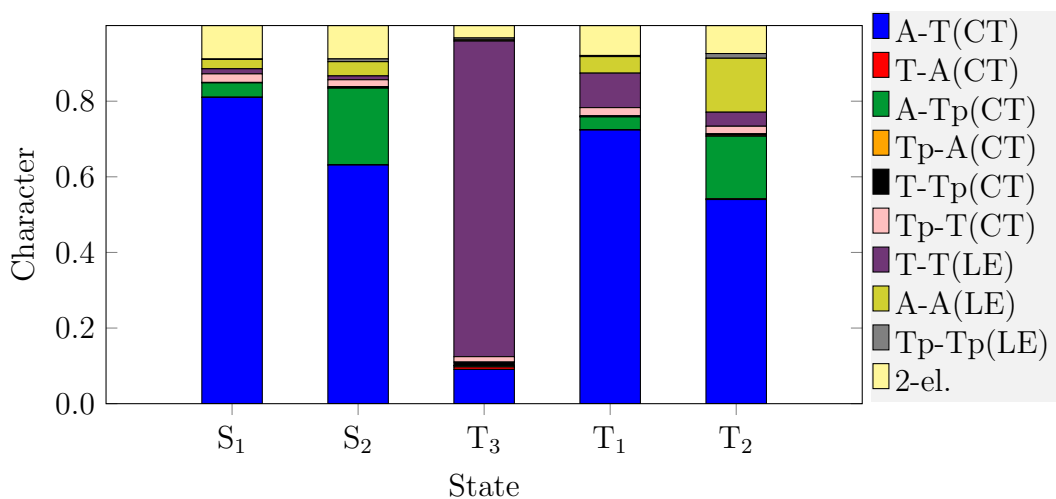


Figure S26: Fragment-based analysis for the vertical singlet and triplet state DFT/MRCI-R2016 wavefunctions at the T<sub>3</sub> geometry in vacuo.

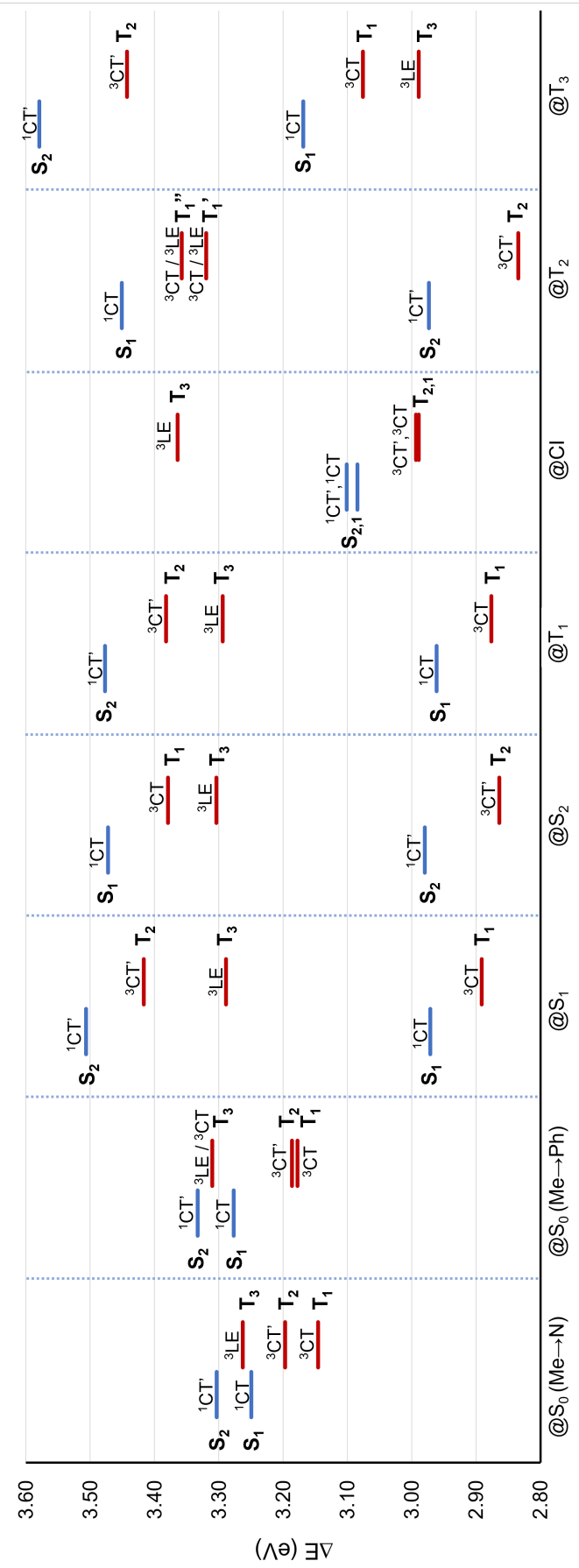


Figure S27: DFT/MRCI excitation energies ( $\Delta E$ , eV) at optimized geometries. CI designates the conical intersection between the T<sub>1</sub> and T<sub>2</sub> PESs. The S<sub>0</sub> energy of the slightly more stable (Me $\rightarrow$ Ph) conformer has been chosen as common origin.

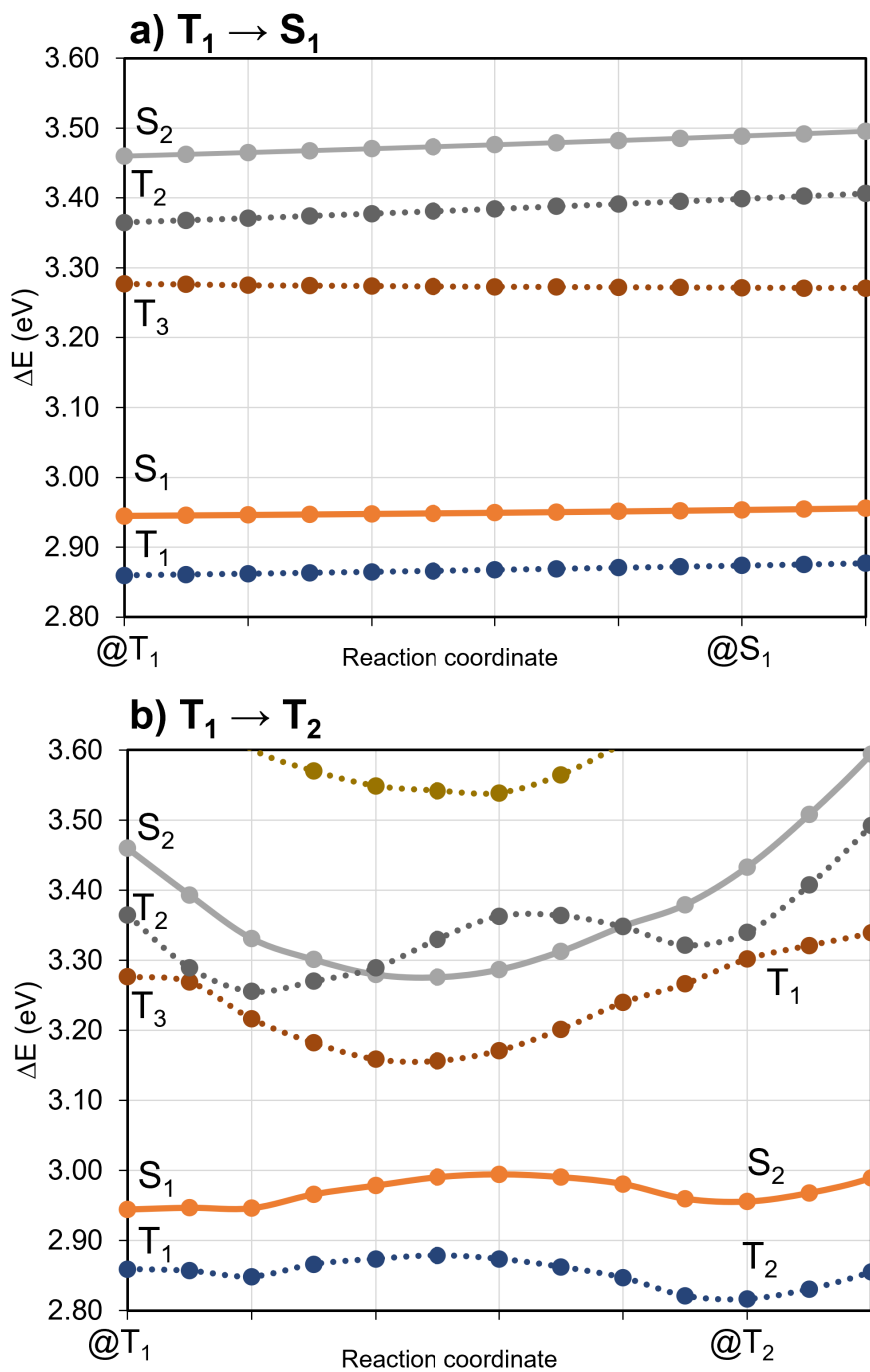


Figure S28: DFT/MRCI energy profiles along linear interpolated pathways (LIPs) between target electronic state minima. Dashed lines correspond to triplet state PESs while solid lines correspond to singlet states.

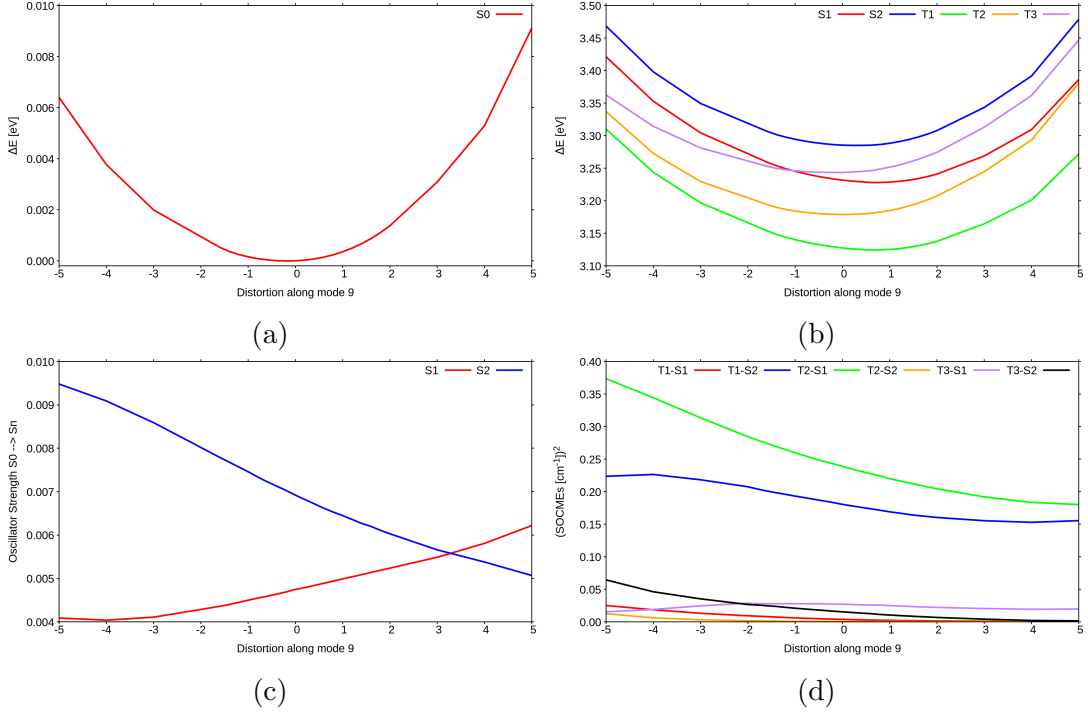


Figure S29: Scan along vibrational mode 9: (a) Relative DFT/MRCI ground state energy differences w.r.t. the undistorted  $S_0(\text{Me} \rightarrow \text{N})$  geometry, (b) DFT/MRCI excitation energies w.r.t. the ground state energy at the undistorted  $S_0(\text{Me} \rightarrow \text{N})$  geometry, (c) oscillator strengths for the  $S_0 \rightarrow S_1$  and  $S_0 \rightarrow S_2$  absorption processes, (d) sum of the squared SOCMEs for transitions discussed in this study.

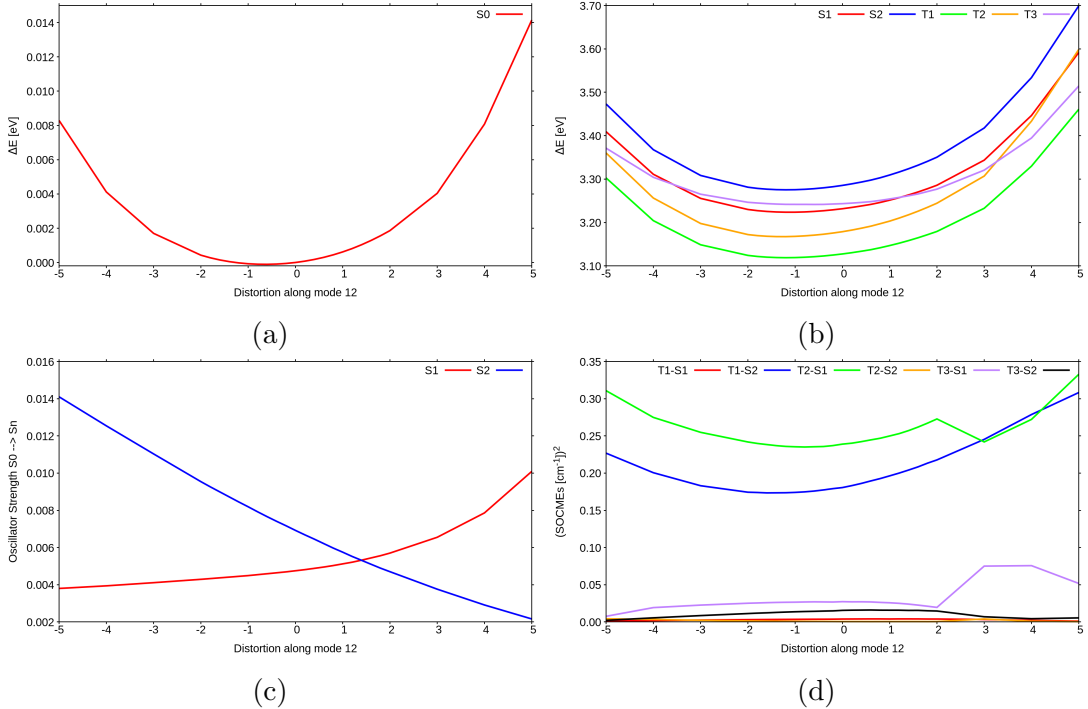


Figure S30: Scan along vibrational mode 12: (a) Relative DFT/MRCI ground state energy differences w.r.t. the undistorted  $S_0(\text{Me} \rightarrow \text{N})$  geometry, (b) DFT/MRCI excitation energies w.r.t. the ground state energy at the undistorted  $S_0(\text{Me} \rightarrow \text{N})$  geometry, (c) oscillator strengths for the  $S_0 \rightarrow S_1$  and  $S_0 \rightarrow S_2$  absorption processes, (d) sum of the squared SOCMEs for transitions discussed in this study.

Table S9: PBE0/def2-SV(P) TDDFT vertical excitation energies (including TDA approximation for triplet states) and characterization of low-lying singlet and triplet states of **TpAT-tFFO** calculated at the  $S_0$ (Me $\rightarrow$ N) geometry.

State	$\Delta E$ [eV]	Transition	Character	%
$S_1$	2.78	H $\rightarrow$ L	CT(A $\rightarrow$ T)	89
		H $\rightarrow$ L+1	CT(A $\rightarrow$ T/Tp)	11
$S_2$	2.83	H $\rightarrow$ L+1	CT(A $\rightarrow$ T/Tp)	89
		H $\rightarrow$ L	CT(A $\rightarrow$ T)	11
$T_1$	2.76	H $\rightarrow$ L	CT(A $\rightarrow$ T)	91
$T_2$	2.81	H $\rightarrow$ L+1	CT(A $\rightarrow$ T/Tp)	91
$T_3$	3.33	H-6 $\rightarrow$ L	LE(T/Tp)	22
		H-5 $\rightarrow$ L	LE(T/Tp)	19
		H-5 $\rightarrow$ L+1	LE(T/Tp)	11

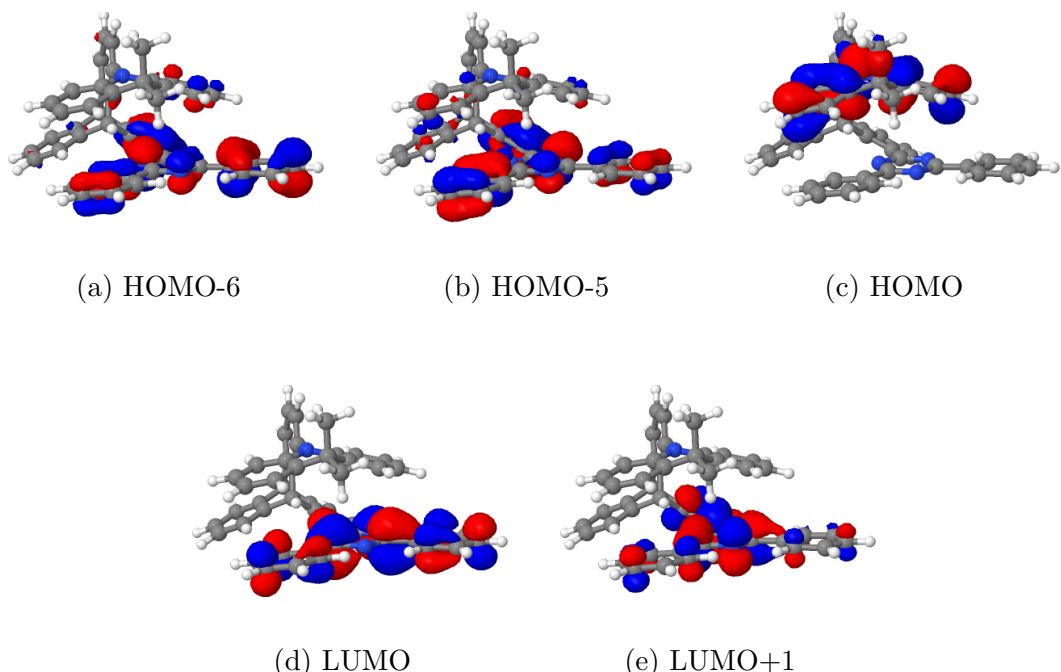


Figure S31: PBE0 molecular orbitals (cutoff 0.03) at the  $S_0$ (Me $\rightarrow$ N) geometry in vacuo.

Table S10: LC- $\omega$ PBE/6-31+G(d) ( $\omega = 0.1664$ ) TDDFT vertical excitation energies (including TDA approximation for triplet states) and characterization of low-lying singlet and triplet states of **TpAT-tFFO** calculated at the  $S_0(\text{Me} \rightarrow \text{N})$  geometry.

State	$\Delta E$ [eV]	Transition	Character	%
$S_1$	2.96	H $\rightarrow$ L	CT (A $\rightarrow$ T)	56
		H $\rightarrow$ L+1	CT (A $\rightarrow$ T/Tp)	42
$S_2$	3.03	H $\rightarrow$ L+1	CT (A $\rightarrow$ T/Tp)	55
		H $\rightarrow$ L	CT (A $\rightarrow$ T)	40
$T_1$	2.93	H $\rightarrow$ L	CT (A $\rightarrow$ T)	62
		H $\rightarrow$ L+1	CT (A $\rightarrow$ T/Tp)	34
$T_2$	3.00	H $\rightarrow$ L+1	CT (A $\rightarrow$ T/Tp)	61
		H $\rightarrow$ L	CT (A $\rightarrow$ T)	32
$T_3$	3.33	H-5 $\rightarrow$ L	LE(A/Tp)	21
		H-6 $\rightarrow$ L	LE(A/Tp)	20

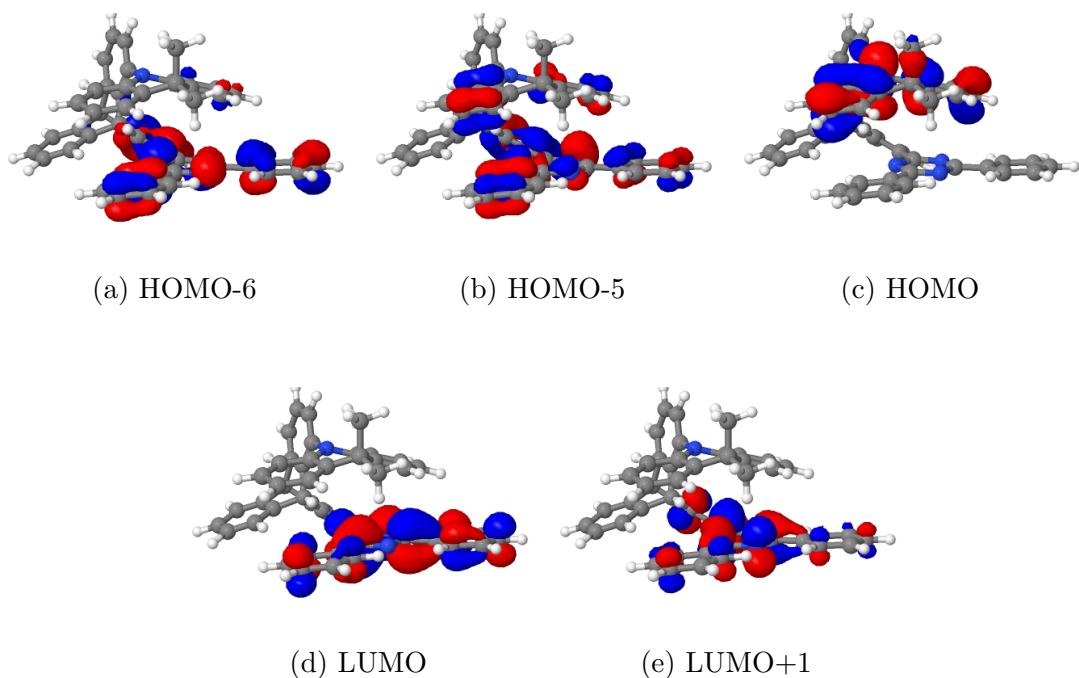


Figure S32: LC- $\omega$ PBE ( $\omega = 0.1664$ ) molecular orbitals (cutoff 0.03) at the  $S_0(\text{Me} \rightarrow \text{N})$  geometry in vacuo.

Table S11: PBE0/def2-SV(P) TDDFT vertical excitation energies (including TDA approximation for triplet states) and characterization of low-lying singlet and triplet states of **TpAT-tFFO** calculated at the  $S_0$ (Me $\rightarrow$ Ph) geometry.

State	$\Delta E$ [eV]	Transition	Character	%
$S_1$	2.83	H $\rightarrow$ L+1	CT(A $\rightarrow$ T/Tp)	53
		H $\rightarrow$ L	CT(A $\rightarrow$ T)	46
$S_2$	2.87	H $\rightarrow$ L	CT(A $\rightarrow$ T)	53
		H $\rightarrow$ L+1	CT(A $\rightarrow$ T/Tp)	46
$T_1$	2.81	H $\rightarrow$ L	CT(A $\rightarrow$ T)	63
		H $\rightarrow$ L+1	CT(A $\rightarrow$ T/Tp)	35
$T_2$	2.84	H $\rightarrow$ L+1	CT(A $\rightarrow$ T/Tp)	63
		H $\rightarrow$ L	CT(A $\rightarrow$ T)	34
$T_3$	3.34	H-6 $\rightarrow$ L	LE(A/Tp)	30
		H-5 $\rightarrow$ L+1	LE(A/Tp)	30
		H-4 $\rightarrow$ L	CT(A $\rightarrow$ T)	10

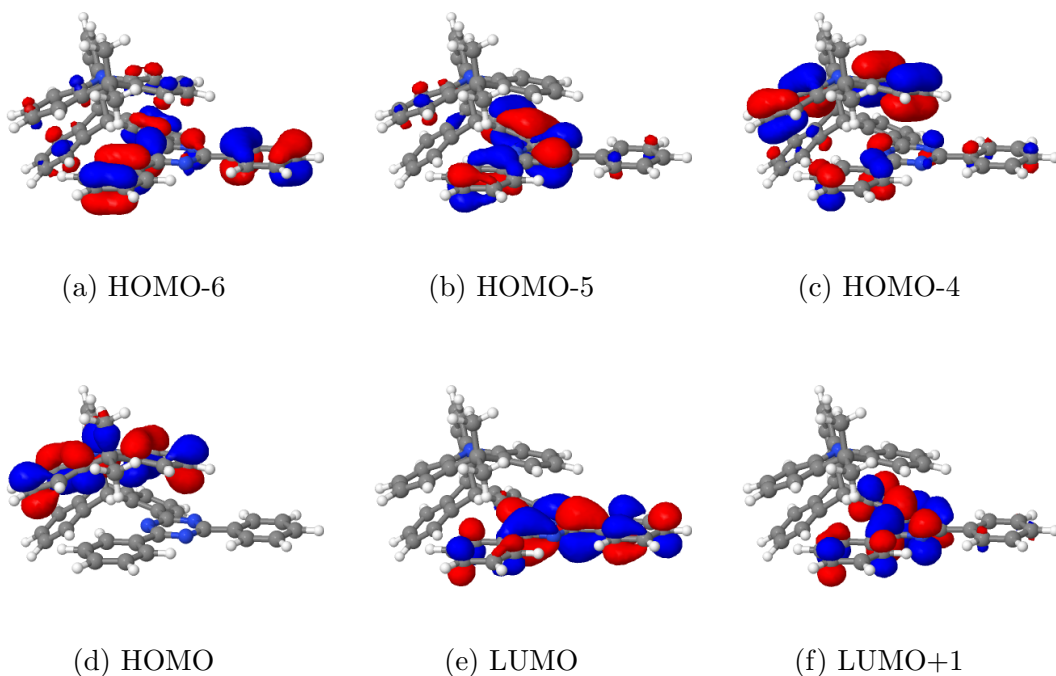


Figure S33: PBE0 molecular orbitals (cutoff 0.03) at the  $S_0$ (Me $\rightarrow$ Ph) geometry in vacuo.

Table S12: LC- $\omega$ PBE/6-31+G(d) ( $\omega = 0.1664$ ) TDDFT vertical excitation energies (including TDA approximation for triplet states) and characterization of low-lying singlet and triplet states of **TpAT-tFFO** calculated at the  $S_0$ (Me→Ph) geometry.

State	$\Delta E$ [eV]	Transition	Character	%
$S_1$	3.01	H → L+1	CT (A→T/Tp)	55
		H → L	CT (A→T)	41
$S_2$	3.12	H → L	CT (A→T)	52
		H → L+1	CT (A→T/Tp)	41
$T_1$	2.99	H → L	CT (A→T)	47
		H → L+1	CT (A→T/Tp)	46
$T_2$	3.07	H → L+1	CT (A→T/Tp)	45
		H → L	CT (A→T)	40
$T_3$	3.35	H-5→L+1	LE(A/Tp)	28
		H-6→L	LE(A/Tp)	21

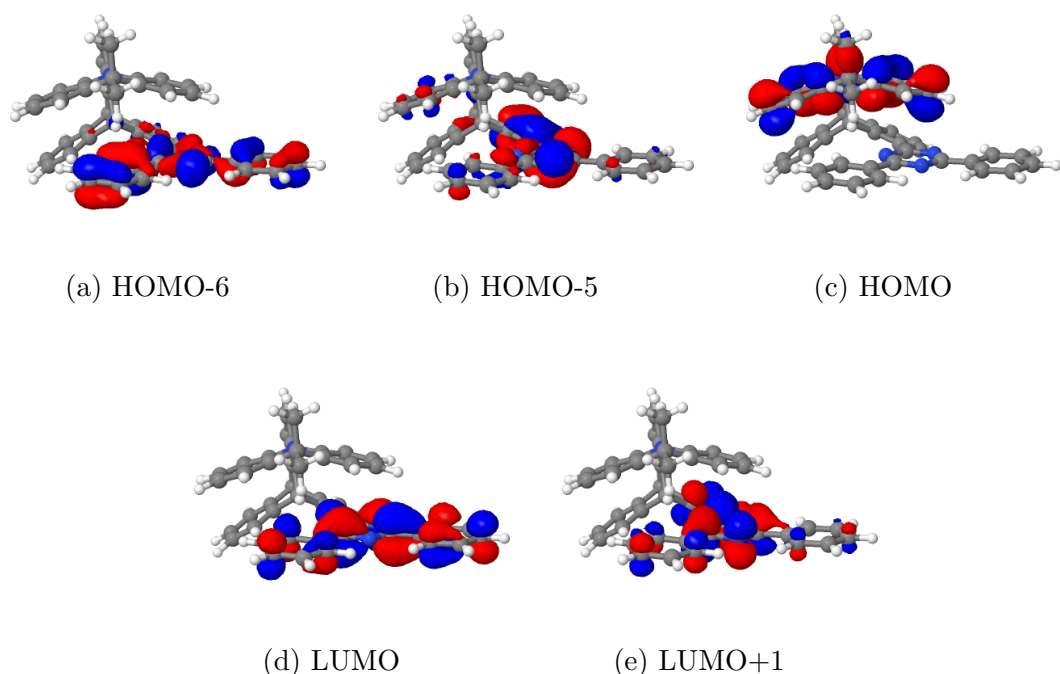


Figure S34: LC- $\omega$ PBE ( $\omega = 0.1664$ ) molecular orbitals (cutoff 0.03) at the  $S_0$ (Me→Ph) geometry in vacuo.

Table S13: PBE0/def2-SV(P) Adiabatic TDDFT excitation energies of low-lying singlet and triplet states of **TpAT-tFFO** (including TDA approximation for triplet states). Zero-point vibrational energy corrections were computed at the (TD)DFT level of theory.

State	$\Delta E$ [eV]	Transition	Character	%	ZPVE
S <sub>1</sub>	2.47	H → L	CT	99.8	-0.11
S <sub>2</sub>	2.49	H → L+1	CT'	99.1	-0.12
T <sub>1</sub>	2.45	H → L	CT	99.4	-0.11
T <sub>2</sub>	2.45	H → L+1	CT'	97.3	-0.12
T <sub>3</sub>	3.09	H-2→L	LE	38.3	+0.04
		H-4→L		17.2	
		H-5→L		15.4	

Table S14: FC rate constants (direct ISC/rISC, s<sup>-1</sup>) between low-lying singlet and triplet state minima of **TpAT-tFFO**. Values smaller than 1 s<sup>-1</sup> have been omitted.

State	ISC (20 K)	ISC (300 K)	rISC (20 K)	rISC (300 K)
S <sub>1</sub> (CT)↔T <sub>1</sub> (CT)	$9.8 \times 10^3$	$8.7 \times 10^4$	—	$5.2 \times 10^3$
S <sub>1</sub> (CT)↔T <sub>2</sub> (CT')	$3.0 \times 10^2$	$2.9 \times 10^5$	—	$9.1 \times 10^2$
S <sub>1</sub> (CT)↔T <sub>3</sub> (LE)	—	$9.5 \times 10^3$	$5.0 \times 10^6$	$2.2 \times 10^6$
S <sub>2</sub> (CT')↔T <sub>1</sub> (CT)	—	$8.6 \times 10^4$	—	$4.2 \times 10^3$
S <sub>2</sub> (CT')↔T <sub>2</sub> (CT')	$1.3 \times 10^5$	$5.3 \times 10^5$	—	$2.6 \times 10^3$
S <sub>2</sub> (CT')↔T <sub>3</sub> (LE)	—	$3.5 \times 10^2$	$7.3 \times 10^4$	$1.2 \times 10^5$

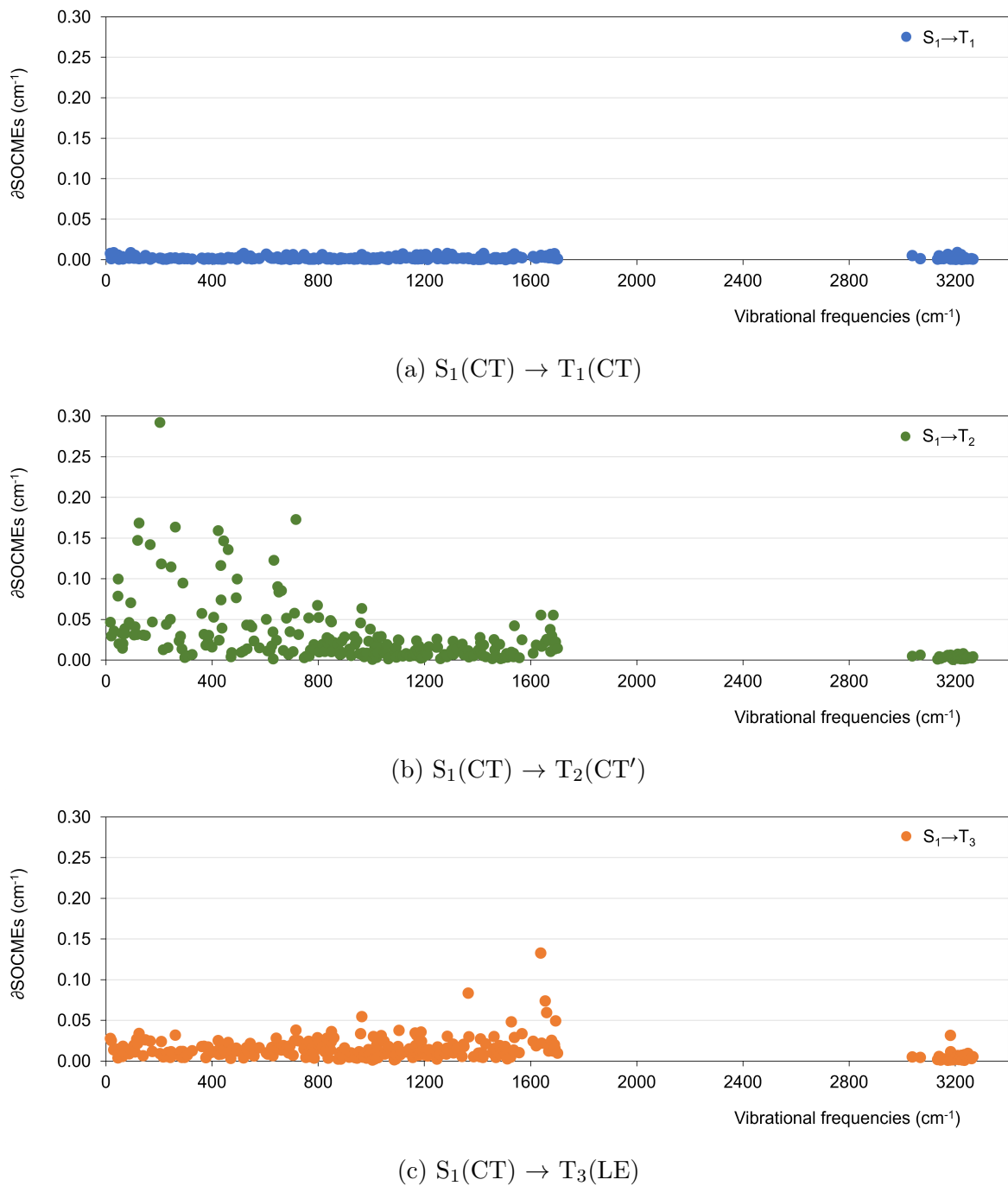


Figure S35: Important coupling vibrational normal modes calculated at the  $S_1$  minimum of **TpAT-tFFO**.

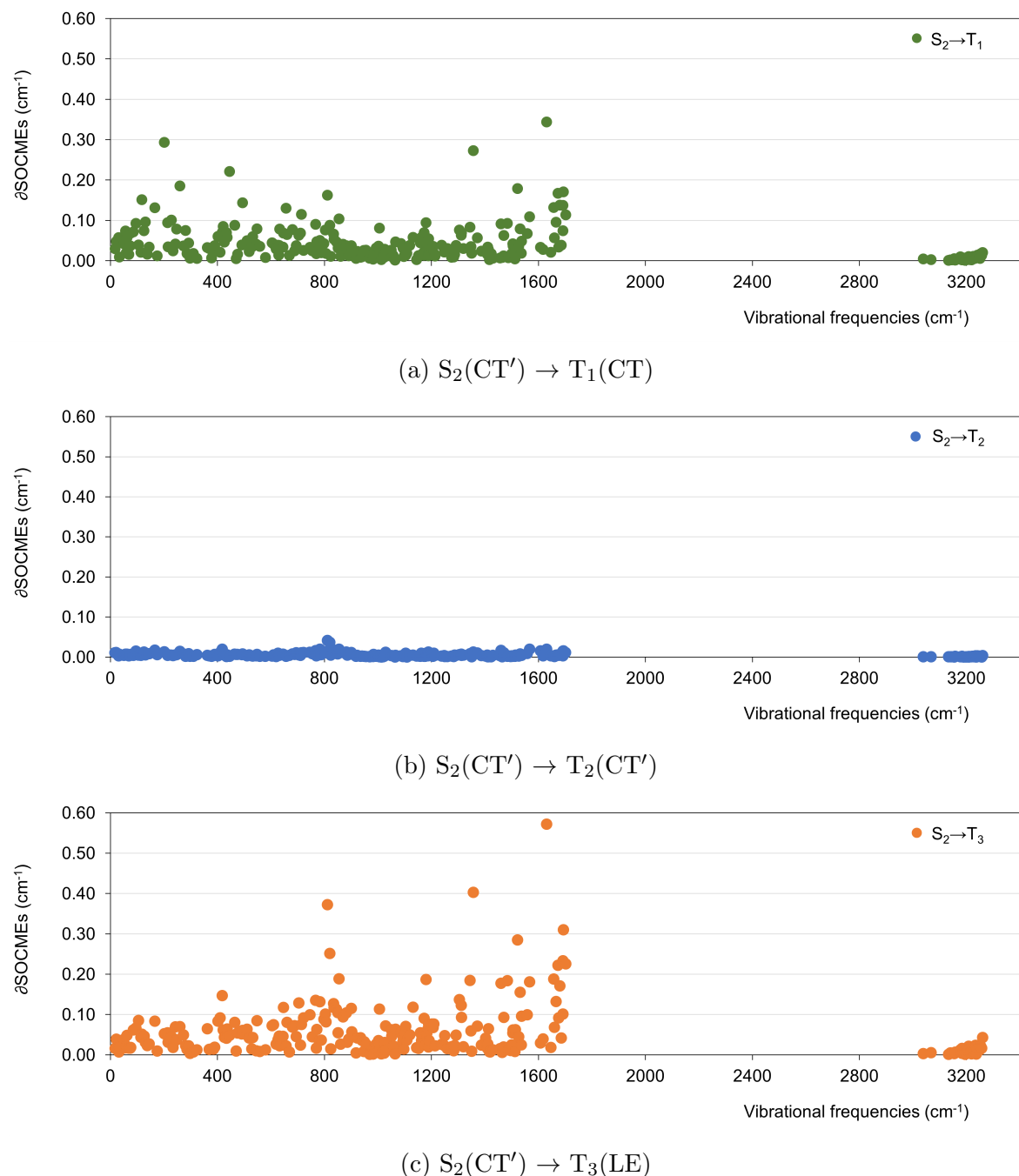
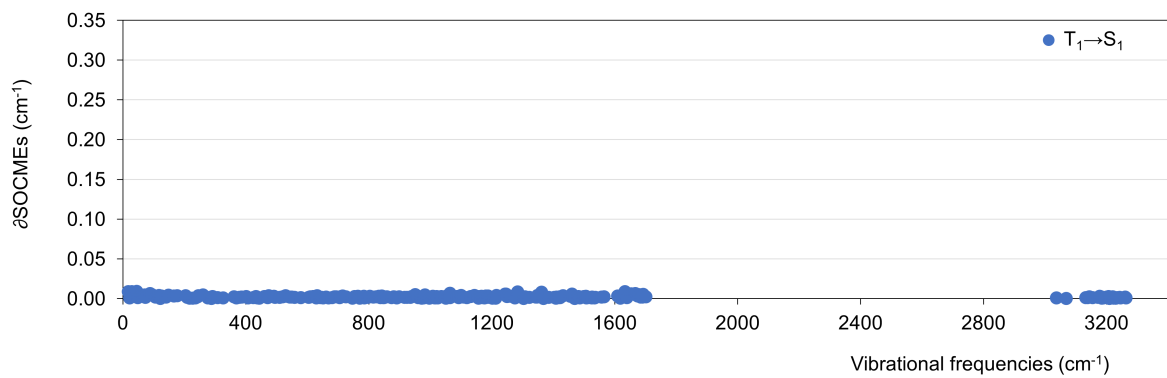
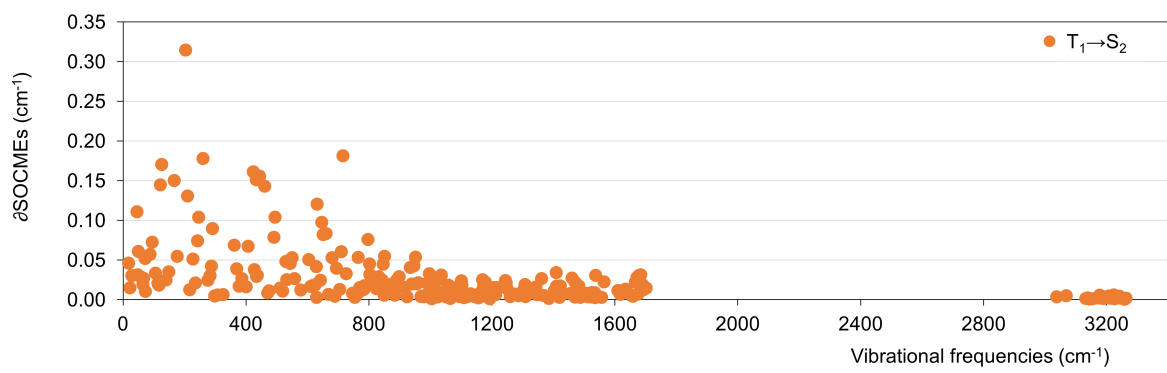


Figure S36: Important coupling vibrational normal modes calculated at the  $S_2$  minimum of **TpAT-tFFO**.

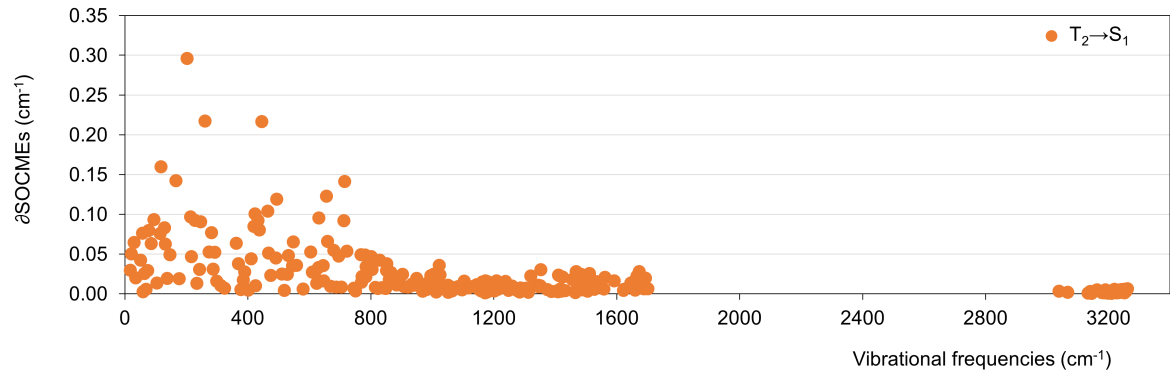


(a)  $T_1(\text{CT}) \rightarrow S_1(\text{CT})$

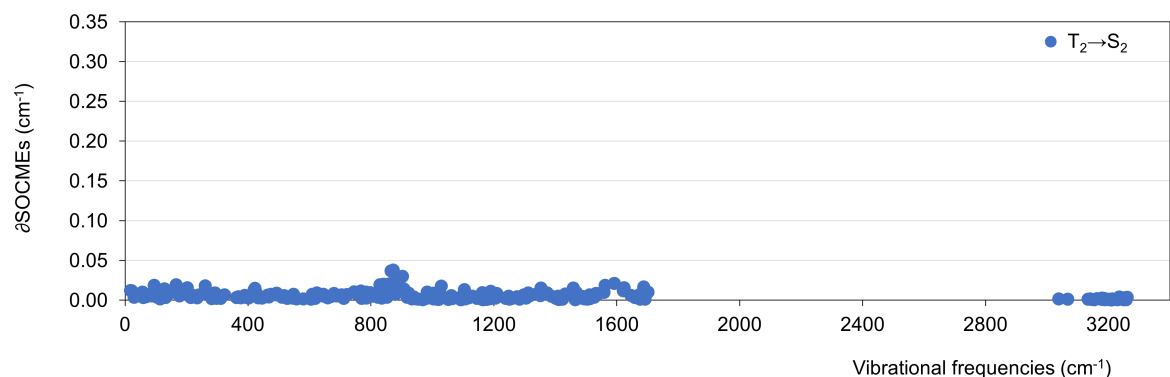


(b)  $T_1(\text{CT}) \rightarrow S_2(\text{CT}')$

Figure S37: Important coupling vibrational normal modes calculated at the  $T_1$  minimum of **TpAT-tFFO**.

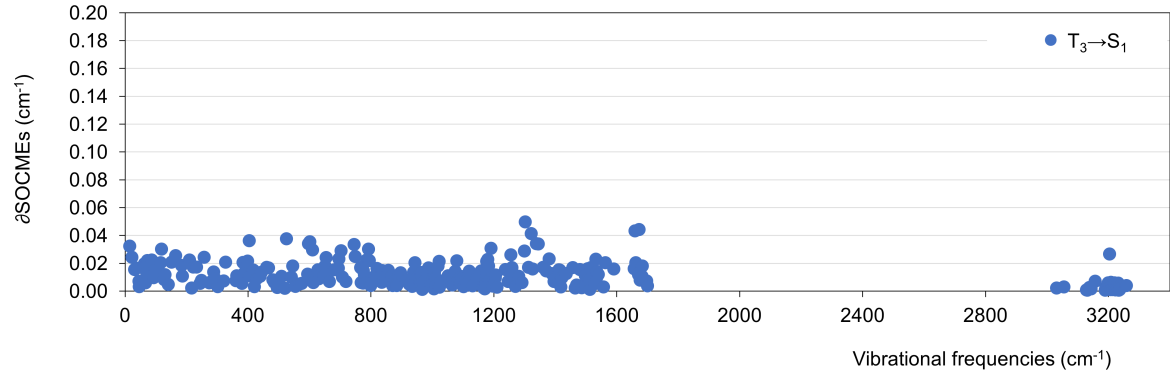


(a)  $\text{T}_2(\text{CT}') \rightarrow \text{S}_1(\text{CT})$

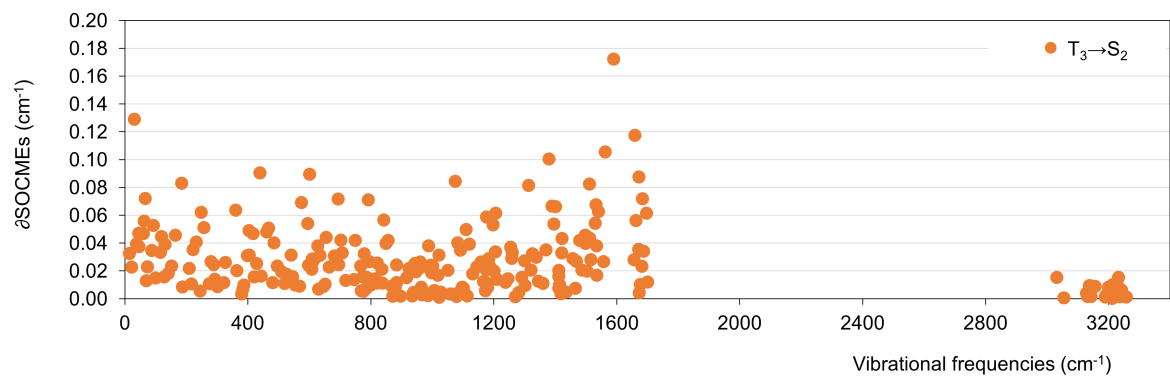


(b)  $\text{T}_2(\text{CT}') \rightarrow \text{S}_2(\text{CT}')$

Figure S38: Important coupling vibrational normal modes calculated at the  $\text{T}_2$  minimum of **TpAT-tFFO**.



(a)  $T_3(\text{LE}) \rightarrow S_1(\text{CT})$



(b)  $T_3(\text{LE}) \rightarrow S_2(\text{CT}')$

Figure S39: Important coupling vibrational normal modes calculated at the  $T_3$  minimum of **TpAT-tFFO**.

Table S15: FC-HT rate constants (direct and vibronic ISC,  $\text{s}^{-1}$ ) at 300 K with shifted potentials in the range of 20 and 170 meV between low-lying singlet and triplet state minima of **TpAT-tFFO**.

State	20 meV	50 meV	80 meV	110 meV	140 meV	170 meV
$S_1(\text{CT}) \rightarrow T_1(\text{CT})$	$4.2 \times 10^6$	$1.4 \times 10^6$	$1.1 \times 10^6$	$7.4 \times 10^5$	$9.6 \times 10^5$	$8.9 \times 10^5$
$S_1(\text{CT}) \rightarrow T_2(\text{CT}')$	$6.0 \times 10^4$	$1.0 \times 10^5$	$1.6 \times 10^5$	$2.4 \times 10^5$	$3.4 \times 10^5$	$4.6 \times 10^5$
$S_1(\text{CT}) \rightarrow T_3(\text{LE})$	$8.6 \times 10^5$	$4.5 \times 10^5$	$2.1 \times 10^5$	$9.0 \times 10^4$	$3.6 \times 10^4$	$1.4 \times 10^4$
$S_2(\text{CT}') \rightarrow T_1(\text{CT})$	$4.1 \times 10^4$	$6.9 \times 10^4$	$1.1 \times 10^5$	$1.6 \times 10^5$	$2.3 \times 10^5$	$3.2 \times 10^5$
$S_2(\text{CT}') \rightarrow T_2(\text{CT}')$	$2.8 \times 10^7$	$9.8 \times 10^6$	$5.9 \times 10^6$	$1.1 \times 10^7$	$7.3 \times 10^6$	$4.3 \times 10^6$
$S_2(\text{CT}') \rightarrow T_3(\text{LE})$	$8.8 \times 10^4$	$4.8 \times 10^4$	$2.4 \times 10^4$	$1.1 \times 10^4$	$3.8 \times 10^3$	$5.3 \times 10^2$

Table S16: FC-HT rate constants (direct and vibronic rISC,  $\text{s}^{-1}$ ) at 300 K with shifted potentials in the range of 20 and 170 meV between low-lying singlet and triplet state minima of **TpAT-tFFO**.

State	20 meV	50 meV	80 meV	110 meV	140 meV	170 meV
$S_1(\text{CT}) \leftarrow T_1(\text{CT})$	$2.6 \times 10^6$	$3.6 \times 10^5$	$5.8 \times 10^4$	$1.5 \times 10^4$	$5.3 \times 10^3$	$1.7 \times 10^3$
$S_1(\text{CT}) \leftarrow T_2(\text{CT}')$	$3.9 \times 10^4$	$2.1 \times 10^4$	$1.0 \times 10^4$	$4.6 \times 10^3$	$2.0 \times 10^3$	$8.6 \times 10^2$
$S_1(\text{CT}) \leftarrow T_3(\text{LE})$	$1.4 \times 10^6$	$2.2 \times 10^6$	$3.3 \times 10^6$	$4.6 \times 10^6$	$5.9 \times 10^6$	$7.3 \times 10^6$
$S_2(\text{CT}') \leftarrow T_1(\text{CT})$	$3.3 \times 10^4$	$1.7 \times 10^4$	$7.9 \times 10^3$	$3.6 \times 10^3$	$1.6 \times 10^3$	$6.5 \times 10^2$
$S_2(\text{CT}') \leftarrow T_2(\text{CT}')$	$1.7 \times 10^7$	$2.0 \times 10^6$	$3.7 \times 10^5$	$2.1 \times 10^5$	$4.6 \times 10^4$	$8.2 \times 10^3$
$S_2(\text{CT}') \leftarrow T_3(\text{LE})$	$1.1 \times 10^5$	$1.9 \times 10^5$	$3.1 \times 10^5$	$4.6 \times 10^5$	$6.6 \times 10^5$	$9.1 \times 10^5$